Miocene geochronology and stratigraphy of western Anatolia: Insights from new Ar/Ar dataset

Bora Uzel [a,*], Klaudia Kuiper [b], Hasan Sözbilir [a], Nuretdin Kaymakci [c], Cornelis G. Langereis [d], Katharina Boehm [b]

[a] Dokuz Eylül University, Department of Geological Engineering, TR-35160 İzmir, Turkey
[b] Vrije Universiteit Amsterdam, Department of Earth Sciences, 1081-HV Amsterdam, the Netherlands
[c] Middle East Technical University, Department of Geological Engineering, TR-06531 Ankara, Turkey
[d] Utrecht University, Fort Hoofddijk Paleomagnetic Laboratory, 3584CD Utrecht, the Netherlands

ARTICLE INFO

ABSTRACT

Understanding the dynamic evolution of orogenic belts and intra-continental basins depend on field-based (tectono-) stratigraphic observations paired with geochronologic data such as $^{40}Ar/^{39}Ar$ analyses. Independent dating of tectono-stratigraphic units is a crucial tool to place them in a broader framework. In this study, we focus on the geodynamic development of western Anatolia, with an emphasis on the timing and progression of volcanism along the İzmir-Balıkesir Transfer Zone (İBTZ). We present 36 new $^{40}Ar/^{39}Ar$ ages of both volcanic complexes/domes and volcanic rocks coevally emplaced within Miocene sediments from western Anatolian extensional basins. In combination with existing ages from the literature and paleontological records from Miocene basin in-fills, we build an improved and integrated stratigraphic framework for the region. Our results show a remarkable break in volcanism from this area during the Langhian (15.97–13.82 Ma), encompassing a major unconformity in the İBTZ, and a pulse in the exhumation of metamorphic core complexes in western Anatolia. Hence we attribute this magmatic pause to the tectonic reorganization and change in the partitioning of extensional deformation between Cycladic and Menderes core complexes, facilitated by the acceleration of roll-back of African oceanic lithosphere below western Anatolia.

© 2019 Elsevier B.V. All rights reserved.

1. Introduction

Dating is one of the fundamental tools in geology to determine the timing, duration, and rates of geological processes (e.g. Krijgsman et al., 1999; Kuiper et al., 2004; Hüsing et al., 2009; De Leeuw et al., 2010). Geochronology plays a crucial role in understanding the geodynamic evolution of western Anatolia, where complex geological processes related to continental collision, oceanic subduction, crustal thickening, metamorphism and magmatism are important in the temporal and spatial evolution of syn-convergence compression and/or extension (Şengör and Yılmaz, 1981; Şengör, 1987; Okay and Tüysüz, 1999; Ring et al., 1999; Bozkurt and Oberhänsli, 2001; Candan et al., 2001; Sözbilir, 2001, 2002, 2005; van Hinsbergen, 2010). Since the Mesozoic, Western Anatolia has undergone active deformation due to the convergence of the African and Eurasian plates. The pattern of deformation is affected by processes occurring at the edge of the slab (Fig. 1; Şengör et al., 1985; Bozkurt, 2001). In the region, two large-scale plate tectonic processes operated simultaneously: i) subduction of the African plate below the Eurasian plate and roll-back of the subducted slab below the Aegean region with respect to Eurasia (e.g. Le Pichon and Angelier, 1979; Meulenkamp et al., 1988; van Hinsbergen et al., 2005; van Hinsbergen et al., 2010; Biryol et al., 2011), and ii) westward escape of the Anatolian Block along the North and East Anatolian fault zones (Dewey and Şengör, 1979; Şengör et al., 1985; Westaway, 1994). The subduction and slab rollback gave way to the development of several of late Cenozoic basins (e.g. Gediz and Buyuk Menderes grabens) formed above the Cycladic (CCC) and the Menderes metamorphic core complexes (MCC), exhumed along detachment faults (e.g., Bozkurt and Park, 1994).

During the Cenozoic, the differential deformation between the CCC and MCC has been accommodated at lithospheric scale by the İBTZ (Ring et al., 1999; Sözbilir et al., 2011; Uzel et al., 2013, 2015; Uzel and Sözbilir, 2008) and Mid Cycladic Lineament (MCL; Morris and Anderson, 1996; Avigad et al., 1998; Walcott and White, 1998; Tirel et al., 2009; Gessner et al., 2013; Philippon et al., 2014). The exact timing, deformation style, and underlying processes of exhumation of the core complexes with respect to activity in the İBTZ are still widely debated. Therefore, we dated volcanic rocks within the İBTZ, which have recorded the extensional history of core complex evolution in the region. Our new $^{40}Ar/^{39}Ar$ age data will provide a more detailed perspective on understanding Miocene volcanism and a more accurate temporal control on geological events along the İBTZ, as well as the extensional processes acting in the upper crust in western Anatolia.
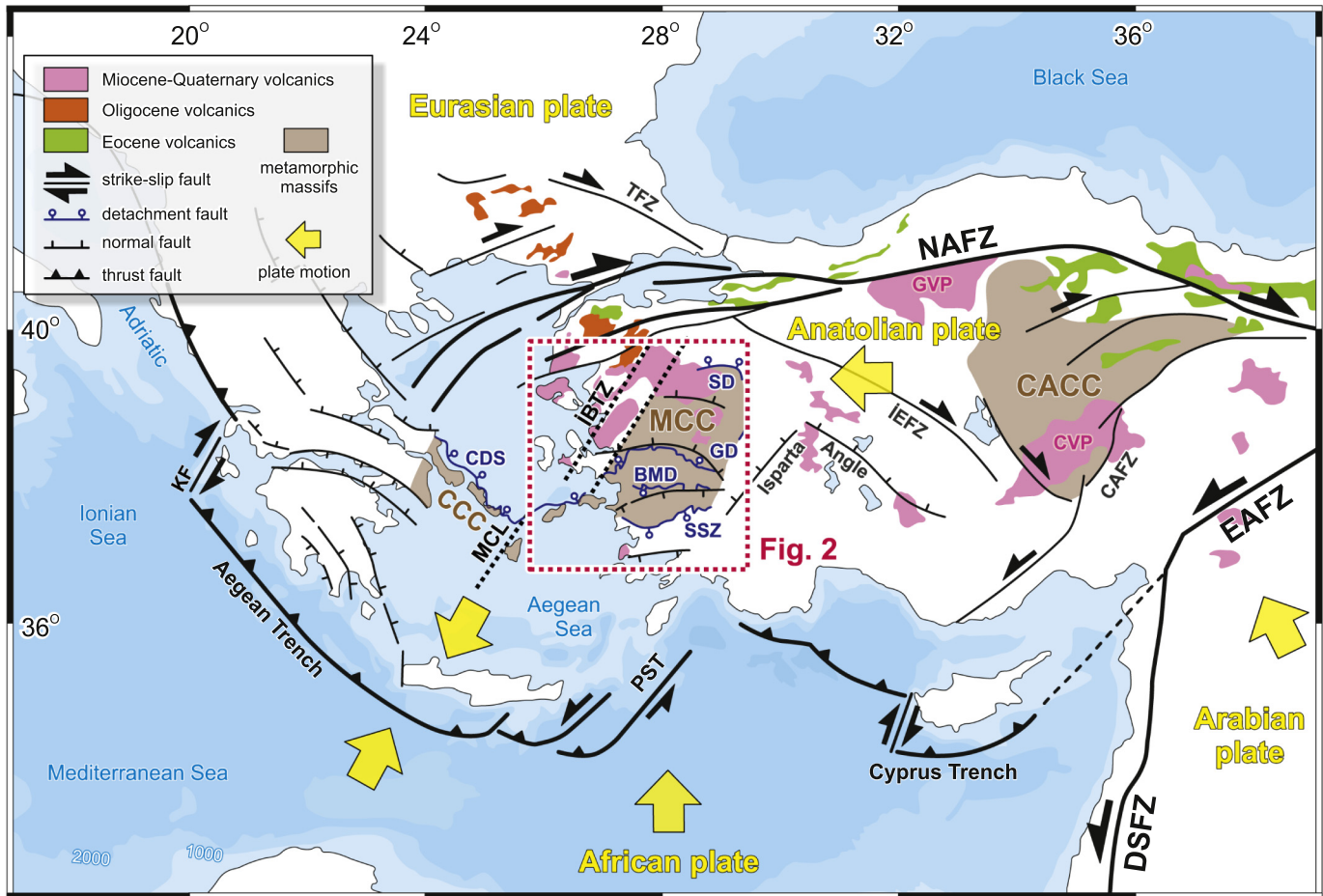

Fig. 1. Simplified tectonic map showing the plate tectonic configuration and distribution of the major neotectonic elements and Cenozoic volcanic rocks exposed on the Anatolian Plate. GVP, Galatian Volcanic Province; CVP, Central Anatolian Volcanic Province; DSFZ, Dead Sea Fault Zone; EAFZ, East Anatolian Fault Zone; NAFZ, North Anatolian Fault Zone; CAFZ, Central Anatolian Fault Zone; PST, Pliny-Strabo Trench; TFZ, Thrace Fault Zone; KF, Kefalonia Fault; İEFZ, İnönü-Eskişehir Fault Zone; SD, Simav Detachment; GD, Gediz Detachment; BMD, Büyük Menderes Detachment; SSZ, Southern Shear Zone; CDS, Cycladic Detachment System; İBTZ, İzmir-Balıkesir Transfer Zone; MCL, Mid Cycladic Lineament (simplified from Şengör et al., 1985; Barka, 1992; Bozkurt, 2001; Koçyiğit and Özaçar, 2003; Biryol et al., 2011; and MTA, 2002, Geological Map of Turkey, scale 1:500.000). Large yellow arrows indicate relative plate motion directions w.t.r. Eurasia. Locations of the main metamorphic core complexes (CCC, Cycladic Core Complex; MCC, Menderes Core Complex; CACC, Central Anatolian Crystalline Complex) are also shown (simplified from Ring et al., 2001; Lefebvre et al., 2012).

Moreover, the combination of this new dataset with the published ages and paleontological records in the literature will help to interpret the Cenozoic tectonics of the Aegean region.

2. Geological setting

2.1. Tectonic framework

Western Anatolia is dominated by E–W trending late Cenozoic extensional basins bounded by basin parallel detachments and high-angle normal faults (e.g. Bozkurt, 2000, 2001; Bozkurt and Park, 1994; Bozkurt and Sözbilir, 2004, 2006; Çiftçi and Bozkurt, 2010; Koçyiğit et al., 1999; Sözbilir, 2001) and NE-SW trending so-called cross-grabens (Şengör et al., 1985). The detachment faults, which are kinematically linked to the crustal-scale metamorphic core complexes and the Cenozoic basins, form the most prominent features of western Anatolia (e.g. Hetzel et al., 1995; Bozkurt and Oberhänsli, 2001; Gessner et al., 2001; Işık and Tekeli, 2001; Ring et al., 2003; Işık et al., 2003; Uzel et al., 2013; Philippon et al., 2014). They are associated with the domal uplift of the footwall block and the formation of asymmetric supradetachment basins in the hangingwall block (Fig. 1). These structures are also associated with NE–SW trending basins that are partly controlled by NE-SW striking strike-slip faults that have been active since the Early Miocene (Kaya, 1981; Kaya et al., 2004, 2007; Ocakoğlu et al., 2004, 2005; Özkaymak et al., 2013; Sözbilir et al., 2011; Sümer

et al., 2013; Uzel et al., 2013, 2017; Uzel and Sözbilir, 2008). The İzmir-Balıkesir Transfer Zone (İBTZ) is a major NE-SW striking fault zone delimiting the western margins of the E-W grabens and is transferring the loci of extensional strain between Menderes and Cycladic core complexes (Uzel et al., 2013, 2015). The İBTZ has developed as a transtensional shear zone and controlled some of the NE–SW trending Miocene basins (Kaya, 1981; Ring et al., 1999; Sözbilir et al., 2011; Uzel et al., 2017).

2.2. Miocene stratigraphy

Various nomenclature has been established for the Miocene lithostratigraphic record of western Anatolia. Although Miocene sedimentary deposition in the MCC (within graben basins) is relatively continuous (Çiftçi and Bozkurt, 2009; Emre, 1996), within the İBTZ, Miocene stratigraphy is characterized by two primary volcano-sedimentary sequences separated by a major angular unconformity, named here as lower sequence and upper sequence (Uzel et al., 2012, 2013, 2017). Current geochronological data based on biostratigraphy (Ünay et al., 1995; Akgün et al., 1995; Ünay and Göktas, 1999; Sarıca, 2000; Kaya et al., 2007; de Bruijn et al., 2006; Kaya et al., 2007) and limited and partly imprecise radio-isotope data (Borsi et al., 1972; Ercan et al., 1996) indicate that the lower sequence is early Miocene, and the upper sequence is middle-late Miocene. The lower sequence deposits start with alternations of reddish to grayish brown conglomerates,

gray sandstone, and greenish-gray mudstone that grades upwards into sandstone-shale alternations (e.g. Kaya, 1981; Uzel et al., 2012). It laterally and vertically passes into an alternation of white to brown lacustrine limestone and claystone. The lower sequence is intensively deformed, yielding many folds, faults, and slumps (Kaya et al., 2004, 2007; Uzel et al., 2012, 2013). During the deposition of the lower sequence in the early Miocene, several volcanic units are extensively emplaced as magmatic domes, dikes, lava flows (Figs. 2 and 3; Kaya, 1981; Genç et al., 2001; Uzel and Sözbilir, 2008; Uzel et al., 2012; Sümer et al., 2013).

The lower sequence is also exposed within the Gediz, Küçük Menderes and Büyük Menderes grabens (above the MCC) with similar lithologic characteristics: the base consists of angular boulder conglomerates, followed by sandstones and mudstones including organic-rich laminated mudstones and/or coal levels (İztan and Yazman, 1990; Sözbilir and Emre, 1996; Ediger et al., 1996; Çiftçi and Bozkurt, 2009; Şen and Seyitoğlu, 2009: Emre et al., 2011). In these areas, the lower sequence contains mammal fossils corresponding to the mammal zones MN2, MN3 and MN4 ranging from 21.7–16.4 Ma (Figs. 2 and 3; Seyitoğlu and Scott, 1996; Ediger et al., 1996; ages for mammal zones from Gradstein et al., 2012).

The upper sequence was deposited in a similar stratigraphic configuration along the İBTZ, but is slightly less deformed (e.g., Uzel et al., 2013). The base level of the upper sequence includes reddish-to

brownish-gray, conglomerates derived from both pre-Miocene and Miocene lower sequence rocks (Kaya, 1981; Uzel et al., 2012, 2017). In the upper part of the sequence, conglomerates usually pass into alternations of sandstone-mudstone and some limestone layers. Light yellow to whitish brown carbonates of late Miocene age conformably overlie the clastic units, representing the top of the upper sequence (Kaya, 1981). A second phase of smaller scale volcanism, compared to previous phase, occurred during the deposition of the upper sequence (Fig. 2).

Outside the İBTZ, the upper sequence rocks above the MCC are mainly composed of red to gray colored conglomerate and sandstone alternations including limestone lenses (İztan and Yazman, 1990; Sözbilir and Emre, 2011; Ediger et al., 1996; Şen and Seyitoğlu, 2009: Emre et al., 2011). The upper sequence contains the MN6–13 mammal zones spanning the period of 14.2 to 5.3 Ma (Fig. 3; Seyitoğlu and Scott, 1996; Ediger et al., 1996; Şan, 1998; Yazman et al., 1998; Koçyiğit et al., 1999; Ünay and Göktas, 1999; Sarıca, 2000; ages for mammal zones from Gradstein et al., 2012). Remarkably, the graben basins do not record widespread volcanic activity during the (middle-) late Miocene, but the footwalls of the basins have been intruded by plutonic rocks (Turgutlu and Salihli Granites on Figs. 2 and 3). Some studies suggest that the Miocene deposition within the grabens lying above the MCC is continuous (e.g. Çiftçi and Bozkurt, 2009; Koçyiğit et al., 1999; Şen and Seyitoğlu, 2009), whereas other studies suggest that the contact between the lower and upper sequences at the eastern side of the İBTZ
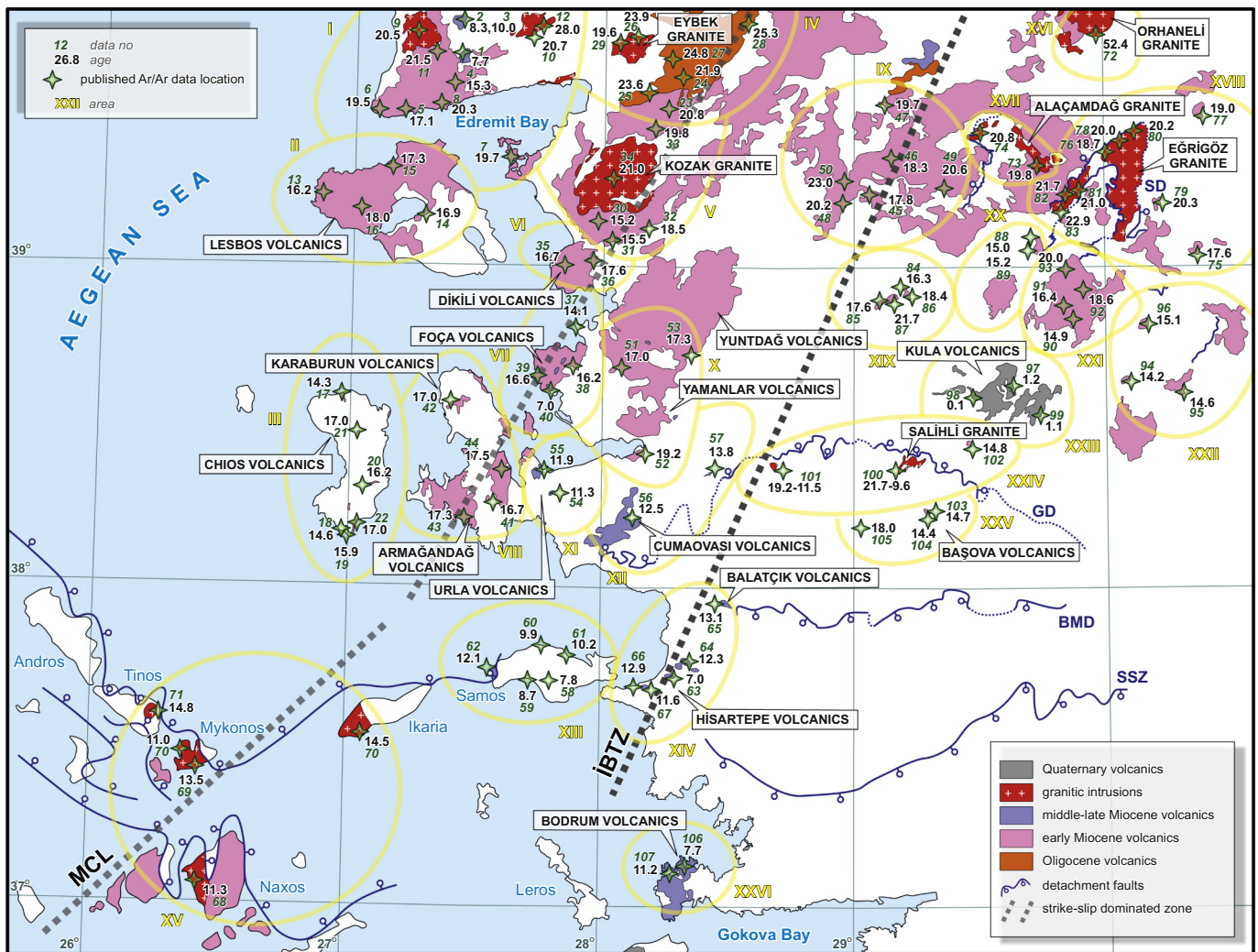

Fig. 2. Simplified geological map showing the main distribution of the Cenozoic magmatic rocks in western Anatolia with their available radio-isotope age data from the literature. Yellow (blue) numbers show sub-areas (data number). See Table 1 for details and related references of data. İBTZ, İzmir–Balıkesir Transfer Zone; MCL, Mid-Cycladic Lineament.
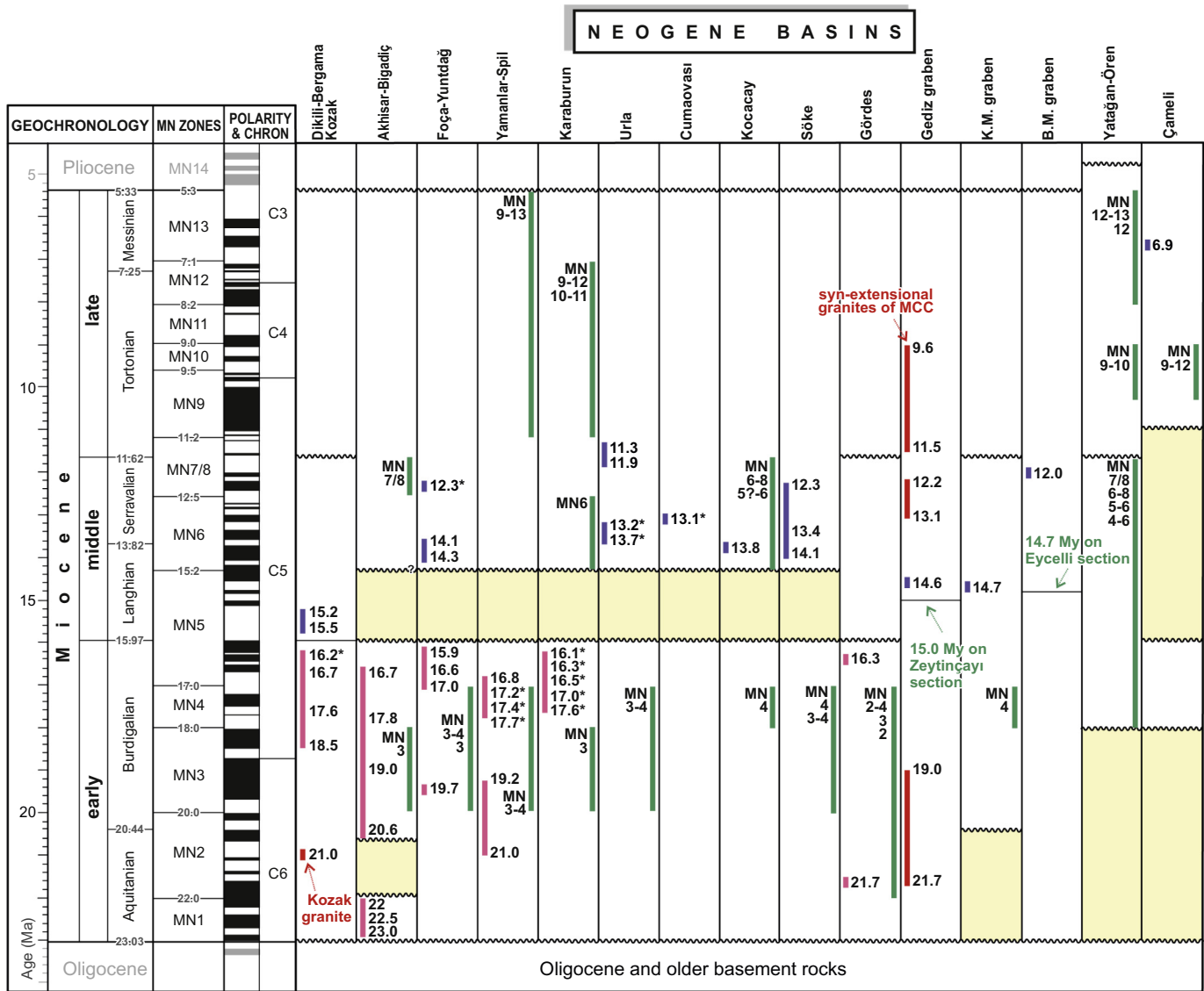
Fig. 3. Stratigraphical correlation of the Cenozoic basins in the İzmir Balıkesir Transfer Zone (İBTZ). Pink, red, and purple bars (with numbered ages) are referring to age distributions of early Miocene volcanism, middle-late Miocene volcanism, and granitic intrusions, respectively; *age data from this study; green bar is mammal age records.

was interrupted by a middle Miocene unconformity (e.g. Ediger et al., 1996; İztan and Yazman, 1990; Yilmaz et al., 2000).

2.3. Miocene magmatism

The main Cenozoic magmatic events in western Anatolia occurred in three distinct time intervals: (i) Oligocene, (ii) Miocene, and (iii) Quaternary (e.g. Borsi et al., 1972; Ercan et al., 1995; Aldanmaz et al., 2000; Erkül et al., 2005a; Kaymakci et al., 2007; Altunkaynak and Genç, 2008; Helvacı et al., 2009; Altunkaynak et al., 2010; Karaoğlu et al., 2010; Ersoy et al., 2012b; Uzel et al., 2017). Here, we focus on Miocene magmatism, encompassing early and middle-late Miocene volcanism (Fig. 2). Miocene volcanism is widespread north of the MCC and along the western side of the İBTZ. The main early Miocene volcanic centers along the İBTZ are exposed around the Yuntdağ, Yamanlar, Armağandağ, Karaburun, Foça, Dikili, and Kozak areas (Fig. 2). Early Miocene volcanic rocks are classified as basalts (Karaburun), andesites, dacite and latite (Yuntağ, Dikili, Armağandağ), phonolite, trachyte and rhyolites (Foça, Yuntağ).The late Miocene volcanism dominantly has a high-K calc-alkaline character (Fig. 2; Akay and Erdoğan, 2004; Erkül

et al., 2005a; Karacık et al., 2007, Karacık and Genç, 2013; Helvacı et al., 2009; Ersoy et al., 2012a).

During the middle-late Miocene, magmatic activity continued in the Foça, Cumaovası and Urla regions and is preserved as small basaltic (e.g. Ovacık, Yağcılar, Yarantepe), andesitic (Foça), rhyolitic lava flows and domes (Urla, Cumovası, Foça), as well as pyroclastic rocks in the middle-late Miocene basins (e.g. Helvacı et al., 2009; Altunkaynak et al., 2010; Karacık and Genç, 2013). This middle-late Miocene volcanism is less voluminous than the early Miocene volcanic activity. In map view, the middle-late Miocene volcanic centers lie mostly parallel to the major NE–SW trending faults of the İBTZ (Fig. 2). For example, in the Cumaovası basin, the volcanic centers and outcrops are aligned in the NNE–SSW direction, forming the 'central volcanics' of this basin (Genç et al., 2001; Uzel and Sözbilir, 2008). In addition, Aldanmaz et al. (2000) also reported that late Miocene alkaline volcanism has generally formed within a NE- and NW-trend.

Miocene magmatism also produced widespread granitic plutons such as the Kozak, Evciler, Eybek, Alaçamdağ, Eğrigöz, Koyunoba, Salihli, and Cyclades (Fig. 2) and likely lasted until the late Miocene in western Anatolia (Table 1). These intrusions are mostly described as granodiorites, quartz diorites, and monazites (Altunkaynak and Genç, 2008;

Table 1
Detailed information about published age data from the western Anatolia. Please see Fig. 2 for their distribution.

Area	Data No	Location	Lithology/location	Method	Mineral	Age (Ma)	Calibration standard[a]; error propagation	Reference
I	1	Biga Peninsula	Basalt	Ar/Ar - step heating (plateau)	Groundmass	7.65 ± 0.36	unknown; ±2SD	Kaymakçı et al. (2007)
	2		Basalt, basanite	K/Ar	Whole rock	8.32 ± 0.19	NA; ±1σ	Aldanmaz et al. (2000)
	3		Basalt (Kızılköy)	Ar/Ar - step heating (plateau)	Groundmass	11.16 ± 0.21	unknown; ±2SD	Kaymakçı et al. (2007)
	4		Ignimbrite	K/Ar	Whole rock	15.3 ± 0.3	NA; unknown	Kaymakçı et al. (2007)
	5		Ignimbrite (Tamos)	K/Ar	Groundmass	17.1 ± 0.6	NA; age uncertainty estimate ±3.5%	Borsi et al. (1972)
	6		Dyke (Baba B.)	K/Ar	Biotite	19.5 ± 0.7	NA; age uncertainty estimate ±3.5%	Borsi et al. (1972)
	7		Trachyandesite	K/Ar	Whole rock	19.7 ± 0.3	NA; ±1σ	Aldanmaz et al. (2000)
	8		Trachyandesite	K/Ar	Whole rock	20.3 ± 0.6	NA; ±1σ	Aldanmaz et al. (2000)
	9		Rhyolite	K/Ar	Whole rock	20.5 ± 0.5	NA; ±1σ	Aldanmaz et al. (2000)
	10		Granite (Evciler)	Rb/Sr	Biotite	20.7 ± 0.02	NA; unknown	Okay and Tüysüz (1999)
	11		Andesitic lava dome (Ayvacik)	K/Ar	Biotite	21.5 ± 0.8	NA; age uncertainty estimate ±3.5%	Borsi et al. (1972)
	12		Granite (Evciler)	Ar/Ar	Hornblende	28.0 ± 0.1	NA; unknown	Altunkaynak et al. (2012)
II	13	Lesbos	Andesitic dyke (Eresos)	K/Ar	Biotite	16.2 ± 0.6	NA; age uncertainty estimate ±3.5%	Borsi et al. (1972)
	14		Ignimbrite (Vasilika)	K/Ar	Biotite	16.9 ± 0.6	NA; age uncertainty estimate ±3.5%	Borsi et al. (1972)
	15		Basaltic andesite (Agios Nectarios lave)	K/Ar	Whole rock	17.9 ± 0.5	NA; unknown	Pe-Piper et al. (2002)
	16		Andesitic lava flow (Parakoila)	K/Ar	Whole Rock	18.3 ± 0.6	NA; age uncertainty estimate ±3.5%	Borsi et al. (1972)
III	17	Chios	Rhyolite (between Aggi pantes and Kambi)	K/Ar	Whole Rock	14.3 ± 0.7	NA; unknown	Bellon et al. (1979)
	18		Rhyolite (Vroulidia Bay)	K/Ar	Whole Rock	14.6 ± 0.8	NA; unknown	Bellon et al. (1979)
	19		Andesite (Mavra Vorsala)	K/Ar	Whole Rock	15.9 ± 0.8	NA; unknown	Bellon et al. (1979)
	20		Alkaline basalt (NE of Pirgi)	K/Ar	Whole rock	16.2 ± 0.6	NA; unknown	Pe-Piper et al. (1995)
	21		Tuff (SW of Pitious)	K/Ar	Whole Rock	17,0 ± 0.8	NA; unknown	Besenecker, 1973
	22		Rhyolite (Profitis Ilias near Komi)	K/Ar	Whole Rock	17,0 ± 0.8	NA; unknown	Bellon et al. (1979)
IV	23	Eybek	Andesite (Sulutas Tepe)	K/Ar	Hornblende	20.8 ± 0.7	NA; unknown	Krushensky (1976)
	24		Volcanics (Behram)	K/Ar	Whole rock	21.9 ± 0.6	NA; unknown	Ercan et al. (1995)
	25		Andesite (Hallarclar)	K/Ar	Biotite	23.6 ± 0.6	NA; unknown	Krushensky (1976)
	26		Granite (Eybek)[c]	U/Pb - SHRIMP	Zircon	23.94 ± 0.31	NA; ±1σ	Altunkaynak et al. (2012)
	27		Andesite	U/Pb	Biotite	23.9 ± 0.3	NA; unknown	Altunkaynak & Genç (2008)
	28		Andesite	K/Ar	Biotite	19.6 ± 0.4	NA; unknown	Altunkaynak and Genç (2008)
	29		Granite (Eybek)[c]	K/Ar	Hornblende	19.6 ± 1.2	NA; unknown	Delaloye and Bingöl (2000)
V	30	Kozak	Volcanics (Nebiler)	K/Ar	Whole rock basaltic andesite	15.2 ± 0.40	NA; ±1σ	Aldanmaz et al. (2000)
	31		Andesite (Eğrigöl)	K/Ar	Whole rock andesite	15.5 ± 0.30	NA; ±1σ	Aldanmaz et al. (2000)
	32		Volcanics (Yuntdağ); lava dome (Bergama)	K/Ar	Biotite	18.5 ± 0.6	NA; age uncertainty estimate ±3.5%	Borsi et al. (1972)
	33		Tuff	K/Ar	Biotite	19.8 ± 0.3	NA; unknown	Benda et al. (1974)
	34		Granite (Kozak)[c]	K/Ar	Hornblende	21.0 ± 1.7	NA; ±1σ	Boztuğ et al. 2009

Table 1 (*continued*)

Area	Data No	Location	Lithology/location	Method	Mineral	Age (Ma)	Calibration standard[a]; error propagation	Reference
VI	35	Dikili	Volcanics (Yuntdağ); lava flow (M. Seyret)	K/Ar	Biotite	16.7 ± 0.6	NA; age uncertainty estimate ±3.5%	Borsi et al. (1972)
	36		Volcanics (Yuntdağ); lava domes (Bergama Graben)	K/Ar	Biotite	17.6 ± 0.6	NA; age uncertainty estimate ±3.5%	Borsi et al. (1972)
VII	37	Foça	Alkaline Felsic Rocks (Foça)	Ar/Ar - step heating	Plagioclase	14.12 ± 0.95	GA1550 98.8 ± 0.5 Ma; ±1σ	Altunkaynak et al. (2010)
	38		Calc-Alkaline Felsic Rocks (Foça)	Ar/Ar - step heating	Plagioclase	16.22 ± 0.37	GA1550 98.8 ± 0.5 Ma; ±1σ	Altunkaynak et al. (2010)
	39		Calc-Alkaline Felsic Rocks (Foça)	Ar/Ar - fusion	Biotite	16.63 ± 0.84	GA1550 98.8 ± 0.5 Ma; ±1σ	Altunkaynak et al. (2010)
	40		Basalt (Foça basalt)	K/Ar	Groundmass	7.00	NA; unknown	Kissel et al. (1987)
VIII	41	Karaburun	Intrusives (Uzunkuyu)	Ar/Ar - step heating isochron	Groundmass	16.7 ± 0.1	unknown; unknown	Helvacı et al. (2009)
	42		Volcanics (Yaylaköy)	Ar/Ar - step heating isochron	Whole Rock	17.0 ± 0.4	unknown; unknown	Helvacı et al. (2009)
	43		Lava dome (Koca D.)	K/Ar	Whole Rock	17.3 ± 0.6	NA; age uncertainty estimate ±3.5%	Borsi et al. (1972)
	44		Volcanics (Kocadağ)	Ar/Ar - step heating isochron	Whole Rock	17.5 ± 0.1	unknown; unknown	Helvacı et al. (2009)
IX	45	Bigadiç	Andesite (Şahinkaya volcanites)	K/Ar	Hornblende	17.8 ± 0.4	NA; ±1σ	Erkül et al. (2005b)
	46		Trachyte (Bigadiç)	K/Ar	Feldspar	18.3 ± 0.2	NA; unknown	Helvacı and Alonso (2000)
	47		Shoshonite (Gölcük basalt)	Ar/Ar - step heating "plateau"	Groundmass	19.7 ± 0.4	unknown; ±1σ	Erkül et al. (2005a, 2005b)
	48		Rhyolite (Sındırgı volcanites)	K/Ar	Biotite	20.2 ± 0.5	NA; ±1σ	Erkül et al. (2005a, 2005b)
	49		Trachyandesite (Kayırlar volcanites)	K/Ar	Biotite	20.6 ± 0.7	NA; ±1σ	Erkül et al. (2005a, 2005b)
	50		Andesite (Kocaiskan volcanites)	K/Ar	Biotite	23.0 ± 2.8	NA; ±1σ	Erkül et al. (2005a, 2005b)
X	51	Yuntdağ-Yamanlar	Andesite	Rb/Sr	Biotite	17.0 ± 0.3	NA; unknown	Ercan et al. (1996)
	52		Dacite (lava dome Izmir)	K/Ar	Mafic fraction	19.2 ± 0.7	NA; age uncertainty estimate ±3.5%	Borsi et al. (1972)
	53		Tuff	K/Ar	Sanidine	17.3 ± 0.6	NA; age uncertainty estimate ±3.5%	Borsi et al. (1972)
XI	54	Urla[b]	Basalt	K/Ar	Whole Rock	11.3 ± 0.4	NA; age uncertainty estimate ±3.5%	Borsi et al. (1972)
	55		Basalt	K/Ar	Biotite	11.9 ± 0.4	NA; age uncertainty estimate ±3.5%	Borsi et al. (1972)
XII	56	Cumaovası[b]	Alakali rhyolites	Rb-Sr isochron		12.5	NA; unknown	Borsi et al. (1972)
	57		Alakali rhyolites	K/Ar	K-feldspar	13.8 ± 0.4	NA; unknown	Göktaş et al. (2013)
XIII	58	Samos	Basalt (Pagondas)	K/Ar	Whole Rock	7.8 ± 0.5	NA; unknown	Pe-Piper and Piper. (2007)
	59		Rhyolite (Koumeika)	K/Ar	Whole Rock	8.7 ± 0.4	NA; unknown	Pe-Piper and Piper. (2007)
	60		Trachyte (Ambelos)	K/Ar	Whole Rock	9.9 ± 0.3	NA; unknown	Pe-Piper and Piper. (2007)
	61		Rhyolite (Ambelos)	K/Ar	Whole Rock	10.2 ± 0.3	NA; unknown	Pe-Piper and Piper. (2007)
	62		Monzogranitic dyke (Kallithea)	U/Pb - LA-ICP-MS	Zircon (rims)	12.12 ± 0.18	NA; ±2σ	Bolhar et al. (2010)
XIV	63	Söke[b]	Volcanics (Hisartepe)	K/Ar	Whole rock basalt	7.55 ± 0.11	NA; unknown	Ercan et al. (1985)
	64		Volcanics (Hisartepe)	Ar/Ar - step heating	Groundmass	12.31 ± 0.09	FCs 28.201; ±2σ	Sümer et al. (2013)
	65		Dacite (Balatçık)	K/Ar	Whole Rock	13,1 ± 0.6	unknown; unknown	Williamson (1982)
	66		Volcanics (Hisartepe)	Ar/Ar - step heating	Groundmass	12.90 ± 0.10	FCs 28.201; ±2σ	Uzel et al. (2017)
	67		Volcanics (Hisartepe)	Ar/Ar - step heating	Groundmass	11.62 ± 0.08	FCs 28.201; ±2σ	Uzel et al. (2017)
XV	68	Cyclades[c]	Granite (Naxos)	U/Pb - SHRIMP	Zircon	11.3 ± 0.2	NA; ±1SE (youngest age selected)	Keay et al. (2001)
	69		Granite (Mykonos)	U/Pb	Zircon	13.64 ± 0.22	NA; ±2σ	Bolhar et al. (2010)
	70		Granite (Ikaria)	U/Pb	Zircon	11.08 ± 0.22	NA; ±2σ	Bolhar et al. (2010)
	71		Granite (Tinos)	U/Pb - LA-ICP-MS	Zircon	14.6 ± 0.2	NA; ±2σ	Brichau et al. (2007)

Table 1 (continued)

Area	Data No	Location	Lithology/location	Method	Mineral	Age (Ma)	Calibration standard[a]; error propagation	Reference
XVI	72	Orhaneli[c]	Granodiorite (Orhaneli)	Ar/Ar - step heating isochron	Biotite	52.4 ± 1.4	unknown; unknown	Harris et al. (1994)
XVII	73	Alaçamdağ[c]	Granite (Alaçamdağ)	Ar/Ar - step heating isochron	Biotite	19.83 ± 0.06	unknown; unknown	Erkül (2010)
	74		Granite (Alaçamdağ)	Ar/Ar - step heating isochron	Biotite	20.82 ± 0.11	unknown; unknown	Erkül (2010)
XVIII	75	Eğrigöz	Andesite	K/Ar	Biotite	17.6 ± 1.0	NA; unknown	Seyitoğlu et al. (1997)
	76		Granite[c]	Rb/Sr isochron	Biotite, whole rock	18.77 ± 0.19	NA; unknown	Hasözbek et al. (2010)
	77		Rhyolite (Emet)	K/Ar	Biotite	19.0 ± 0.2	NA; unknown	Helvacı and Alonso (2000)
	78		Granite (Alacam)[c]	U/Pb - ID-TIMS	Zircon	20.0 ± 1.4	NA; ±2σ	Hasözbek et al. (2011)
	79		Granite (Alacam)[c]	U/Pb - ID-TIMS	Zircon	20.3 ± 3.3	NA; ±2σ	Hasözbek et al. (2011)
	80		Granite[c]	Ar/Ar	Biotite	20.2 ± 0.3	520.4 Ma; ±1σ	Işık et al. (2004)
	81		Granite[c]	U-Th-Rb	Zircon	21 ±	NA; unknown	Ring and Collins (2005)
	82		Granite (Egrigoz)[c]	U/Pb - ID-TIMS	Zircon	21.7 ± 1.0	NA; ±2σ	Hasözbek et al. (2010)
	83		Granite[c]	Ar/Ar - plateau	Muscovite	22.9 ± 0.5	520.4 Ma; ±1σ	Işık et al. (2004)
XIX	84	Gördes	Central Volcanics	K/Ar	Biotite	16.3 ± 0.5	unknown; unknown	Seyitoğlu et al. (1994)
	85		Acidic tuff in sedimentary infill	Ar/Ar - fusion	Biotite	17.04 ± 0.35	unknown; ±1σ	Purvis et al. (2005)
	86		Central Volcanics	K/Ar	Biotite	18.4 ± 0.8	unknown; unknown	Seyitoğlu et al. (1994)
	87		Acidic tuff in sedimentary infill	Ar/Ar - fusion	Biotite	21.7 ± 0.04	unknown; ±1σ	Purvis et al. (2005)
XX	88	Demirci	Naşa Basalt	K/Ar	Whole rock	15.0 ± 0.3	NA; unknown	Ercan et al. (1996)
	89		Naşa Basalt	K/Ar	Whole rock	15.2 ± 0.3	NA; unknown	Ercan et al. (1996)
XXI	90	Selendi	Andesite (Selendi)	K/Ar	Biotite	14.9 ± 0.6	NA; ±2σ	Seyitoğlu et al. (1997)
	91		Tuff (Selendi)	Ar/Ar - fusion	Feldspar	16.42 ± 0.99	unknown; ±1σ	Purvis et al. (2005)
	92		Lamproite (Kuzayır)	Ar/Ar - step heating total gas	Phlogopite	18.6 ± 0.2	unknown; ±1σ	Ersoy et al. (2008)
	93		Volcanics (Eğreltidağ)	Ar/Ar - step heating plateau	Amphibole	20.0 ± 0.2	unknown; ±1σ	Ersoy et al. (2008)
XXII	94	Uşak	Lamproite alkaline volcanics (Güre)	Ar/Ar - total fusion	Groundmass	14.20 ± 0.12	FCT-3 biotite 27.95 Ma; ±2σ	Innocenti et al. (2005)
	95		Andesite	K/Ar	Whole Rock	14.6 ± 0.3	NA; ±2σ	Seyitoğlu et al. (1997)
	96		Tuff (intercalated in Neogene sediments)	K/Ar	Whole Rock	15.1 ± 0.4	NA; ±2σ	Seyitoğlu et al. (1997)
XXIII	97	Kula	Basalt	Ar/Ar	Amphibole	1.25 ± 0.08	NA; unknown	Westaway et al. (2004)
	98		Basalt	K/Ar	Whole Rock	0.1–0.2	NA; NA	Ercan et al. (1996)
	99		Basalt	K/Ar	Groundmass	1.1 ± 0.04	NA; age uncertainty estimate ±3.5%	Borsi et al. (1972)
XXIV	100	Gediz	Granite (Salihli)[c]	Th/Pb ion microprobe	Monazite	9.6 ± 1.6–21.7 ± 4.5		Catlos et al. (2010)
	101		Granite (Turgutlu)[c]	Th/Pb ion microprobe	Monazite	11.5 ± 0.8–19.2 ± 5.1		Catlos et al. (2010)
	102		Andesite (Toygar)	K/Ar	Whole Rock	14.8 ± 0.4	NA; unknown	Ercan et al. (1996)
XXV	103	Küçük Menderes	Andesite (Başova)	Ar/Ar	Biotite	14.7 ± 0.1	unknown; unknown	Emre and Sözbilir (2005)
	104		Andesite (Başova)	Ar/Ar	Biotite	14.4 ± 0.2	TCR-2 sanidine 28.34 Ma; age uncertainty estimate ±0.2%, ±2σ	Bozkurt et al. (2009)
	105		Tuff	Rb/Sr	Whole Rock	18.0 ± 0.2	NA; unknown	Ercan et al. (1996)
XXVI	106	Bodrum[b]	Basaltic Andesite (Bodrum Volcanics)	K/Ar	Whole Rock	7.8 ± 0.3	unknown; unknown	Robert and Cantagrel (1977)
	107		Bodrum Volcanics	K/Ar	Monazite	11.2 ± ?	unknown; unknown	Pişkin (1980)

[a] Only applicable for Ar/Ar,otherwise NA = not applicable.
[b] Late Miocene volcanic centers.
[c] Granitic intrusions.

Fig. 4. a) Detailed map showing volcanic areas and distribution of sampling locations for ^{40}Ar/^{39}Ar geochronology. Sample codes indicated in gray did not yield reliable age data. b-d) Field photos of selected/representative sample locations: Yamanlar volcanics (b), Ovacık basalt (c), and Foça volcanics. Please note that pink (purple) coded volcanic rocks are belonging lower sequence (upper sequence). Cv, Çandarlı-Dikili volcanics; Yuv, Yuntdağ volcanics; Fv, Foça volcanics; Yav, Yamanlar volcanics; Bb, Beşyol basalt; Kav, Karaburun volcanics; Yv, Yaylaköy volcanics; Kv, Kocadağ volcanics; Av, Armağandağ volcanics; Uv, Urla volcanics; Ob, Ovacık basalt; Yb, Yağcılar basalt; Cv, Cumaovası volcanicsş Al, Aliağa limestone.

Altunkaynak and Yılmaz, 1998, 1999; Hasözbek et al., 2011; Karacık and Yılmaz, 1998; Pe-Piper et al., 2002; Yılmaz, 1989). According to structural studies, the emplacement of granitic plutons is mainly due to the evolution/exhumation of metamorphic core complexes along detachment (e.g. Emre, 1996; Seyitoğlu et al., 1997; Lips et al., 2001; Bozkurt and Sözbilir, 2004Glodny and Hetzel, 2007; Catlos et al., 2010) and transfer faults (Avigad and Ziv, 2001; Pe-Piper et al., 2002; Denèle et al., 2011; Kokkalas and Aydın, 2013).

3. ⁴⁰Ar/³⁹Ar geochronological data

3.1. Sampling and analytical procedure

The thirty-five freshest samples within the İBTZ (Çandarlı, Cumaovası, Karaburun, Urla, Yamanlar, and Yuntdağ) were selected for $^{40}Ar/^{39}Ar$ dating (Fig. 4 and Table 2). The specimens were taken from lava flows (some of them columnar jointed), dikes, and pyroclastic rocks deposited or emplaced during the deposition of Miocene sedimentary rocks. Based on field classification, the rock types range from basalt, basaltic andesite, andesite, dacite, and rhyolite. Mineral separation and $^{40}Ar/^{39}Ar$ dating were performed at the Vrije Universiteit Amsterdam, the Netherlands.

First, all samples were crushed, washed, and sieved. Standard heavy liquid and magnetic separation techniques were applied to bulk fractions of 250–500 μm grain size. Depending on the rock composition, sanidine, biotite, plagioclase, and groundmass fractions were separated. All mineral fractions were handpicked under an optical microscope. Additionally, groundmass fractions were leached in dilute nitric acid for

one hour in an ultrasonic bath. 10–30 mg of material from each sample was wrapped in Al-foil and loaded in a 9 mm ID aluminum vial. Fish Canyon Tuff sanidine or Drachenfels sanidine were loaded at the top and bottom positions and between each set of 3 or 5 samples to monitor the neutron flux. Samples were irradiated in different irradiation batches VU82, VU88, VU92 and VU97 in the High Flux Reactor (Petten, the Netherlands) in the cadmium shielded RODEO P3 position for respectively 12, 12, 1, and 18 h. After irradiation, samples and standards were loaded in 2 mm diameter holes of a copper planchet for single fusion analyses and/or 5 mm diameter holes for incremental heating experiments. Samples were preheated at 250 °C under vacuum before being placed in an ultra-high vacuum extraction line. Samples were heated with a Synrad 48–5 CO_2 continuous-wave laser system, and the gas was analyzed with a Mass Analyzer Products LTD 215–50 noble gas mass spectrometer and in a few cases with a Hiden quadrupole mass spectrometer (Schneider et al., 2009).

Beam intensities were measured in a peak-jumping mode over the mass range 40–36 on a secondary electron multiplier. For data collection, the mass spectrometer is operated with a modified version of standard MAP software. Data reduction was carried out using the ArArCalc software of Koppers (2002). Each analysis was corrected for mass discrimination and system blanks. System blanks were measured every three steps. Mass discrimination was monitored by frequent analysis of $^{40}Ar/^{36}Ar$ air pipette aliquots. The irradiation parameter J-value for each unknown was determined by interpolation using a second-order polynomial fitting between the individually measured standards.

All $^{40}Ar/^{39}Ar$ sample ages were calculated using the decay constants of Min et al. (2000). The age for the Fish Canyon Tuff sanidine neutron

Table 2

Summary of $^{40}Ar/^{39}Ar$ results of this study. MSWD, mean square weighted deviate; N, number of steps included (excluded) in the plateau age; $^{39}Ar_k$ (%), percentage of $^{39}Ar_k$ released by plateau steps. Errors are given at 95% confidence level. Samples indicated in gray did not yield reliable age data. Please see Fig. 4 for distribution of samples. Detailed analytical data provided in supplementary data as Table S2.

Lab ID	Irradiation	Sample ID	Mineral	Method	Fraction (mm)	J value	MSWD	N	$^{39}Ar_k$ (%) in plateau	K/Ca	Weighted mean plateau or fusion age (Ma)	Total gas age (Ma)	Inverse isochron age (Ma)	Inverse isochron intercept
10m0136	VU82-B4	KB01	groundmass	incremental heating	250-500	0.0032419	11.63	7(6)	56.7	0.30 ± 0.03	17.96 ± 0.20	18.30 ± 0.25	16.98 ± 0.36 ✓	425.4 ± 44.6
10m0139	VU82-B7	KB03	groundmass	incremental heating	250-500	0.0031948	1.74	11(2)	92.9	0.18 ± 0.02	16.50 ± 0.16 ✓	16.57 ± 0.14	15.64 ± 1.16	313.1 ± 24.0
10m0138	VU82-B6	KB05	groundmass	incremental heating	250-500	0.0032095	0.58	8(6)	74.4	0.87 ± 0.05	17.55 ± 0.18 ✓	18.05 ± 0.17	17.50 ± 0.52	296.2 ± 6.4
10m0132	VU82-B1	KB08	groundmass	incremental heating	250-500	0.0032958	1.38	7(4)	85.1	0.71 ± 0.05	16.07 ± 0.11 ✓	15.99 ± 0.10	16.01 ± 0.45	302.2 ± 48.2
10m0107	VU82-B8	KB10	sanidine	fusion	400-500	0.0033042	0.35	8(2)		13.0 ± 1.1	13.19 ± 0.08 ✓	13.22 ± 0.08	13.20 ± 0.09	295.1 ± 3.0
10m0133	VU82-B2	KB10	groundmass	incremental heating	250-500	0.0032797	1.49	13(1)	99.0	1.07 ± 0.12	13.22 ± 0.09 ✓	13.26 ± 0.10	13.13 ± 0.11	302.2 ± 5.3
10m0137	VU82-B5	KB14	groundmass	incremental heating	250-500	0.0032259	0.86	10(3)	78.6	0.41 ± 0.05	13.02 ± 0.17 ✓	13.29 ± 0.32	12.78 ± 0.49	298.2 ± 5.3
10m0134	VU82-B3	KB17	groundmass	incremental heating	250-500	0.0032627	0.73	9(4)	87.3	0.21 ± 0.03	15.70 ± 0.99	20.45 ± 2.07	13.69 ± 2.53 ✓	299.1 ± 4.2
10m0184	VU82-B10	KB18	sanidine	fusion	400-500	0.0032975	1.83	17(9)		10.9 ± 5.1	13.13 ± 0.08 ✓	13.90 ± 0.08	13.10 ± 0.09	331.4 ± 43.1
10m0183	VU82-B9	KB19	sanidine	fusion	400-500	0.0033009	1.83	16(6)		36.5 ± 8.2	13.12 ± 0.08 ✓	14.02 ± 0.08	13.14 ± 0.09	259.4 ± 63.0
11m0443	VU88-A3	KB21	sanidine	fusion	400-500	0.0033380	1.81	7(3)		43.3 ± 4.9	16.27 ± 0.11 ✓	16.26 ± 0.10	16.37 ± 0.26	208 ± 274
11m0444	VU88-A4	YM01	feldspar	fusion	250-500	0.0032660	0.60	9(1)		0.33 ± 0.06	17.34 ± 0.05 ✓	16.09 ± 0.36	16.29 ± 1.07	287.3 ± 21.1
11m0484	VU88-A7	YM02	biotite	fusion	250-500	0.0034058	1.4	7(2)		3.70 ± 1.14	17.22 ± 0.04 ✓	17.22 ± 0.09	17.26 ± 0.14	276.7 ± 20.3
11m0485	VU88-A8	YM04	biotite	fusion	250-500	0.0034063	1.29	6(3)		11.9 ± 1.5	17.44 ± 0.10 ✓	17.50 ± 0.09	17.67 ± 0.47	267.0 ± 57.3
11m0488	VU88-A15	YY01	groundmass	incremental heating	250-500	0.0033927	5.12	5(7)	70.4	1.14 ± 0.37	17.74 ± 0.13 ✓	17.58 ± 0.11	17.76 ± 0.21	286.6 ± 60.3
11m0489	VU88-A17	M0813	groundmass	incremental heating	250-500	0.0033815	2.05	8(3)	99.7	0.23 ± 0.01	12.33 ± 0.22 ✓	12.38 ± 0.16	11.43 ± 2.10	304.4 ± 21.8
VU88_A18_1*	VU88-A18	M0819	plagioclase	incremental heating	200-500	0.0033689	1722	10(10)	100	0.11 ± 0.03	100.41 ± 13.39	103.99 ± 0.73	-5.8 ± 5.0	2825 ± 1426
11m0508	VU88-A9	M0821	biotite	fusion	250-500	0.0034063	1.43	13(4)		4.1 ± 0.9	17.24 ± 0.09 ✓	17.07 ± 0.11	17.26 ± 0.09	294.2 ± 1.3
11m0502	VU88-A30	M0822	plagioclase	incremental heating	200-500	0.0033010	0.12	2(9)	65.5	0.088 ± 0.003	17.21 ± 0.18 ✓	17.07 ± 0.15	-	-
11m0506	VU88-A34	M0825	plagioclase	incremental heating	200-500	0.0032772	29.3	3(8)	75.5	0.085 ± 0.006	17.07 ± 0.57	16.97 ± 0.21	15.99 ± 0.54 ✓	530 ± 108
11m0490	VU88-A19	M0828	groundmass	incremental heating	250-500	0.0033689	3.76	3(9)	46.8	0.86 ± 0.10	17.13 ± 0.18 ✓	17.26 ± 0.11	17.60 ± 0.35	280.0 ± 10.6
11m0492	VU88-A20	M0831	groundmass	incremental heating	250-500	0.0033610	2.86	4(8)	53.9	0.82 ± 0.11	19.02 ± 0.13	18.95 ± 0.12	18.79 ± 0.29 ✓	639 ± 388
11m0450	VU88-A10	M0832	biotite	fusion	200-500	0.0034057	1.42	8(2)		11.2 ± 15.3	18.49 ± 0.22 ✓	18.10 ± 0.23	18.45 ± 0.42	296.3 ± 6.6
11m0452	VU88-A12	M0833	biotite	fusion	250-500	0.0034282	1.88	8(2)		5.5 ± 7.7	18.60 ± 0.24 ✓	18.76 ± 0.22	18.33 ± 0.29	304.2 ± 7.1
11m0504	VU88-A32	M0835	plagioclase	incremental heating	250-500	0.0032895	3.89	2(9)	56.7	0.07 ± 0.01	18.19 ± 0.31 ✓	18.02 ± 0.15	-	-
11m0505	VU88-A33	M0836	plagioclase	incremental heating	250-500	0.0032841	1.62	7(4)	99.9	0.07 ± 0.01	18.41 ± 0.17 ✓	18.35 ± 0.16	18.47 ± 0.66	290.7 ± 52.9
11m0453	VU88-A13	M0837	biotite	fusion	250-500	0.0034008	0.19	3(7)		1.8 ± 1.2	18.31 ± 0.17 ✓	17.54 ± 0.13	18.77 ± 1.46	283.1 ± 39.2
11m0493	VU88-A22	M0837	groundmass	incremental heating	250-500	0.0033498	1.79	8(4)	79.5	5.6 ± 0.3	18.30 ± 0.11 ✓	18.23 ± 0.11	18.30 ± 0.12	292.3 ± 20.4
11m0445	VU88-A37	M0838	biotite	fusion	250-500	0.0032610	1.07	6(1)		181 ± 175	18.68 ± 0.11 ✓	18.31 ± 0.11	18.69 ± 0.16	294.9 ± 4.5
11m0483	VU88-A5	M0838	feldspar	fusion	250-500	0.0034001	0.83	10(0)		0.13 ± 0.03	18.63 ± 0.71 ✓	18.69 ± 0.75	18.82 ± 1.24	279 ± 108
11m0454	VU88-A14	M0840	biotite	fusion	250-500	0.0033981	1.05	8(2)		3.0 ± 1.5	18.62 ± 0.13 ✓	18.57 ± 0.12	18.76 ± 0.34	263.4 ± 75.9
11m0494	VU88-A23	M0840	groundmass	incremental heating	250-500	0.0033444	0.36	4(8)	59.3	0.66 ± 0.15	19.66 ± 0.13 ✓	19.70 ± 0.12	19.69 ± 0.25	285.4 ± 69.1
12m0108	VU92-11L	DEM1	groundmass	incremental heating	250-500	0.0002629	1.55	6(5)	96.1	2.67 ± 0.23	18.51 ± 0.05 ✓	18.50 ± 0.05	18.48 ± 0.07	321.4 ± 42.6
12m0105	VU92A-9L	YUNT5	groundmass	incremental heating	250-500	0.0002630	1.69	5(6)	92	0.52 ± 0.06	17.27 ± 0.07 ✓	17.09 ± 0.07	17.32 ± 0.30	293.6 ± 10.3
12m0104	VU92-8L	YUNT7	groundmass	incremental heating	250-500	0.0002634	0.21	4(7)	79.1	1.85 ± 0.24	18.48 ± 0.05 ✓	18.52 ± 0.16	18.52 ± 0.14	284.3 ± 42.5
12m0103	VU92-7L	YUNT8	groundmass	incremental heating	250-500	0.0002634	1.58	4(7)	85.4	0.37 ± 0.02	17.14 ± 0.08 ✓	16.90 ± 0.07	16.03 ± 1.21	332.7 ± 40.6
12m0110	VU92A-13L	CAN1	groundmass	incremental heating	250-500	0.0002606	0.00	2(12)	50.7	0.35 ± 0.09	21.91 ± 0.34 ✓	51.41 ± 1.09	-	-
12m0109	VU92A-12L	CAN2	groundmass	incremental heating	250-500	0.0002618	1.17	5(6)	96.3	0.36 ± 0.02	16.15 ± 0.07 ✓	16.07 ± 0.07	16.46 ± 0.78	286.0 ± 23.8
12m0106	VU92A-10L	FC02	groundmass	incremental heating	250-500	0.0002630	1.15	4(10)	17.9	0.050 ± 0.006	6.38 ± 1.56 ✓	691 ± 38	8.49 ± 3.17	281.7 ± 19.6

fluence monitor used in the age calculations is 28.201 ± 0.023 Ma (Kuiper et al., 2008). The age for the Drachenfels standard is 25.52 ± 0.08 Ma. Please note that this age is based on the 24.99 ± 0.07 Ma reported in Wijbrans et al. (1995) relative to Taylor Creek Rhyolite of 27.92 Ma, and using the intercalibration factor 1.0112 ± 0.0010 of Renne et al. (1998) and the recommended age of Kuiper et al. (2008) and Min et al. (2000) decay constant, this converts to 25.52 ± 0.08 Ma. Errors are quoted at the 1σ level in the manuscript (Table 2), and all details are given in supplementary data (Table S2). An incremental heating age is accepted as an accurate estimate of the crystallization age when the following criteria are fulfilled: a plateau contains more than 50% of the ^{39}Ar released and is formed by three or more concordant (at the 95% confidence level), contiguous steps. A well-defined isochron should be obtained from the results of the gas fractions in the plateau, while also the ^{40}Ar/^{36}Ar intercept for the trapped argon derived from the isochron should not be significantly different from the atmospheric ratio of 295.5 (Nier, 1950). If no plateau age could be calculated or if the sample includes excess atmospheric argon, an isochron age was determined. For three samples (M0819, FC02, and CAN1), a plateau age could not be calculated because of high amounts of excess argon (Table 2). In the end, 36 ^{40}Ar/^{39}Ar analyses from 32 samples were used for further applications.

3.2. Results

Five samples were collected from the Karaburun area (Fig. 4a). KB01 and KB03 are from the Yaylaköy volcanics; KB05, KB08, and KB21 represent the Kocadağ, Armağandağ, and Foça volcanics, respectively. The groundmass fraction of the samples is used for ^{40}Ar/^{39}Ar dating. Results indicate that the ages of volcanism in the Karaburun area range between 17.96 and 16.07 Ma (Fig. 5 and Table 2). Based on these results, it can be concluded that the Yaylaköy, Kocadağ, Armağandağ, and Foça volcanic events occurred in approximately the same time interval (Fig. 6). In the Urla basin, we highlight results from three volcanic fields that are generally composed of basalts (Fig 4b). From each field, one representative sample was collected, labelled as KB10, KB14, and KB17 (Yağcılar basalt, Urla volcanics, and Ovacık basalt, respectively). The plateau ages of KB14 (13.02 Ma of groundmass) and KB10 (13.19 Ma of sanidine and 13.22 Ma of groundmass) are comparable; however, the plateau age of KB17 (15.70 Ma of groundmass) is substantially older. Field evidence indicates that all of these lava flows belong to the upper sequence, representing the sequences deposited above the mid-Miocene unconformity. This geochronological plateau age of ~15.7 Ma contrasts field evidence suggesting that the lava flows in KB17 site must belong to the lower sequence. However, it should be noted that the 13.69 Ma isochron age of KB17 is in agreement with its stratigraphic position, but more importantly the low ^{40}Ar content (<10%) in this sample suggests that alteration processes may affect the estimated plateau age of sample KB17 (Fig. 5 and Table 2). To compare with the other samples, the sanidine fraction of KB10 was also analyzed. The fusion result yields an age of 13.19 Ma, which fits within the same time span of KB10 and KB14 (Fig. 5).

The samples KB18, KB19, and YY01 were collected from the Cumaovası basin. These samples belong to two different volcanic successions (Fig. 4). YY01 characterizes the Yamanlar volcanics in the lower volcano-sedimentary sequence, and the incremental heating age of the groundmass is 17.74 Ma (Fig 4c and 5), which is in agreement with data in the literature from Borsi et al. (1972; K-Ar data) and Innocenti et al. (2005; Ar/Ar data). Just south of YY01, KB18 and KB19 were collected from the Cumaovası volcanics representing the upper sequence. The calculated sanidine ages (13.13 Ma and 13.12 Ma) are identical to the age results of Urla region (Figs. 2, 5 and Table 2).

Twenty-one sites were dated from the Yamanlar and Yuntdağ area (Fig. 4). The internal structure of these areas is very complex, and field evidence of cross-cutting relationships implies the existence of multiple phases of volcanism, whilst in other areas, lava flows and related

pyroclastics are relatively monotonously emplaced. The samples labeled as YM01, YM02, YM04, M0821, and M0822 characterize the Yamanlar volcanics. The oldest age is 17.44 Ma (biotite age of YM04) obtained from the center of the Yamanlar area, while the youngest is 17.34 Ma (biotite age of YM01). These ages are consistent despite the sampling sitesbeing distributed over a relatively large area (Figs. 4, 5 and Table 2). The Yuntdağ volcanics are the most widespread volcanic rocks in the study area and are aligned in an approximately NE-SW direction. In order to determine the age of various volcanic pulses within this area, samples for ^{40}Ar/^{39}Ar dating were collected from fifteen sites. These samples are labeled as M0813, M0825, M0828, M0831, M0832, M0833, M0835, M0836, M0837, M0838, M0840, DEM1, YUNT5, YUNT7, and YUNT8 (Fig. 4). The lithology of the samples includes basalts, andesites, dacites, and volcanic glass (perlite). Plagioclase, biotite, and groundmass are used for dating. All samples yield ages ranging between 17.13 (groundmass age of M0828) and 19.66 Ma (groundmass age of M0840), apart from sample M0813 (Fig. 5 and Table 2). Surprisingly, the groundmass of sample M0813 collected from the center of Yuntdağ yielded an age of 12.33 Ma. This sample has distinctive characteristics such as columnar jointing, and its olivine-bearing basalt looks similar to the basaltic lava flows from the Urla basin. Therefore, it is concluded that this basalt must belong to the upper sequence of middle-late Miocene age and most probably was emplaced along the NW-trending Güzelhisar fault zone (Uzel et al., 2013). Additionally, some samples were analyzed twice on different materials (biotite and groundmass) to check for consistency. All ages indicate that our results are internally consistent. For example, the isotopic age obtained from biotite minerals and the groundmass for sample M0837 yielded the same ages of 18.30 Ma (Fig. 5 and Table 2).

4. Discussion

4.1. Spatio-temporal characteristics of Miocene magmatism

The present-day distribution of Cenozoic volcanic and depositional centers is mainly controlled by the extensional and transtensional tectonic setting of western Anatolia, including detachment faults (such as Simav, Gediz, and Büyük Menderes detachments) and lithospheric scale zones of weaknesses (İBTZ and MCL), respectively. These tectonic elements were developed during the exhumation of metamorphic core complexes (Menderes and Cyclades) related to the evolution of the Tethys Ocean. Among these elements the İBTZ plays an important role in the localization of eruption centers and in controlling the evolution of transtensional Neogene basins in the region (Akay and Erdoğan, 2004; Erkül et al., 2005a; Ersoy et al., 2014; Genç et al., 2001; Gessner et al., 2013; Kaya, 1981; Uzel et al., 2013). The İBTZ is composed of NE–SW elongated Miocene volcano-sedimentary basins that are dissected by mainly E–W elongated Plio–Quaternary depressions (Uzel and Sözbilir, 2008). Miocene stratigraphy starts at the bottom with an intensely deformed volcano-sedimentary sequence consisting of coal-bearing clastics to carbonates, andesitic to rhyolitic pyroclastics, and lava flows (Fig. 7). The Plio-Quaternary basin-fills are represented by continental alluvial to fluvial deposits and coastal clastics of the Aegean Sea. The Neogene–Quaternary evolution of the zone is characterized by variable wrench-to extension-dominated transtension and has resulted in a complex fault pattern (Sözbilir et al., 2011; Uzel et al., 2013).

Since the 1970s, several geochronological datasets have been published for the volcanic and magmatic centers to constrain the complexity of tectonic events in western Turkey. Methods range from zircon and apatite fission-track, U/Pb laser ablation inductively coupled plasma (LA-ICP-MS), U/Pb thermal ionization mass spectrometry (TIMS), Th-Pb ion microprobe ages, Rb-Sr, K/Ar, and Ar/Ar geochronology. A compilation of relevant literature is given in Table 1 to provide a geochronological overview of western Turkey (Fig. 2). It should be noted that the data reported in some of these studies do not follow current standards (Renne et al., 2009). In some cases, it is unclear if uncertainties are
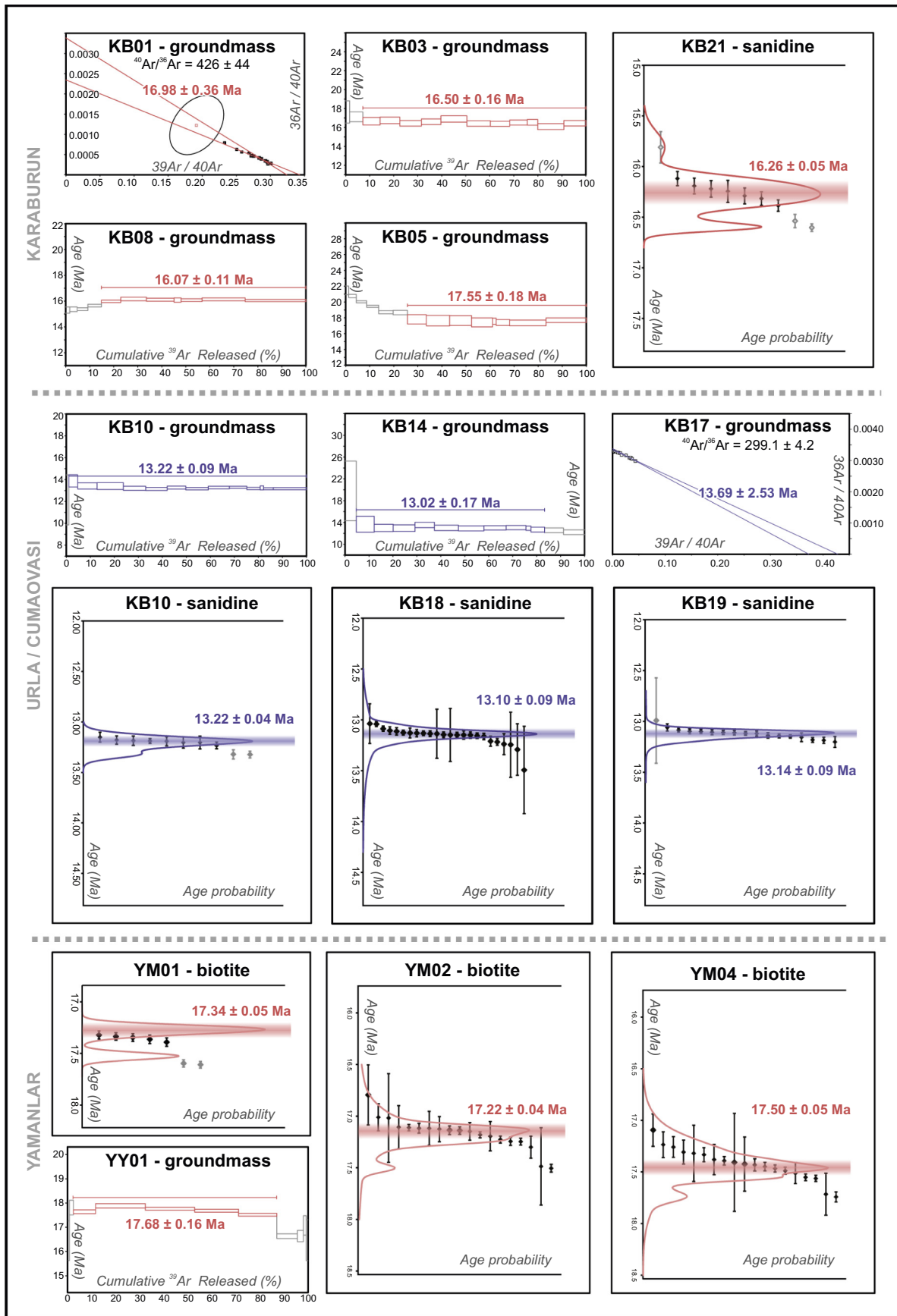
Fig. 5. Incremental heating $^{40}Ar/^{39}Ar$ spectra and/or single fusion analyses of thirty-five samples. The width of the bars/steps represents the 2σ analytical error. Weighted mean (plateau) ages are displayed. For three samples, the inverse isochron diagrams are also shown, because these sample contain excess argon and their isochron age is preferred over their spectrum. Pink and purple colors are referring to early and middle-late Miocene volcanics, respectively.
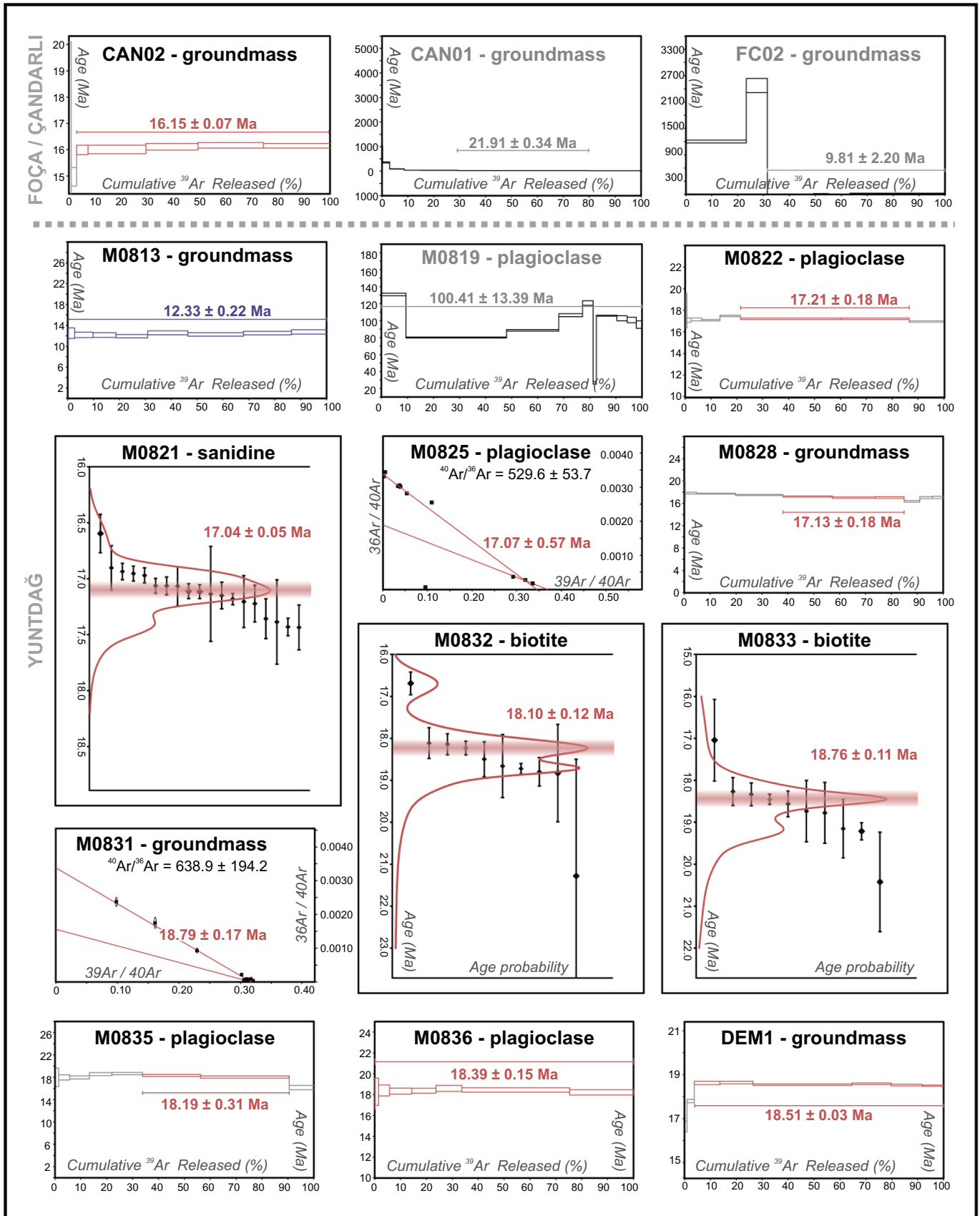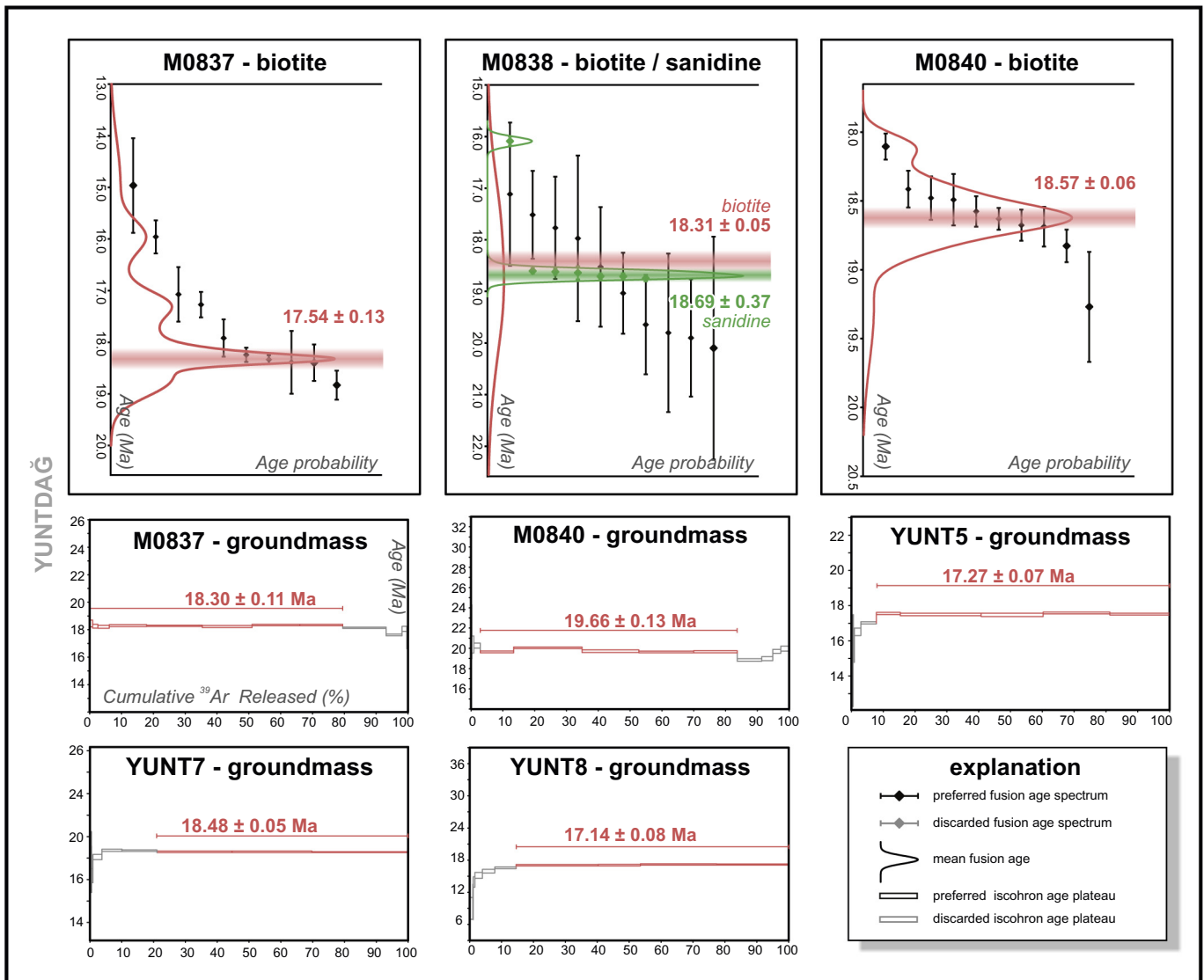
Fig. 5 (*continued*).

Fig. 5 (*continued*).

propagated at 1 or 2 sigma level. In the case of Ar/Ar dating, it is not always specified which age calibration model is used (standard, decay constant and standard age), which decay constant, and what $^{40}K/K$ ratio is used for K/Ar studies. It is also not always possible to assess the quality of data due to the lack of sufficient analytical information (e.g. radiogenic ^{40}Ar yields). Here, we list ages as originally published (without uncertainties in Fig. 2), but emphasize that the associated uncertainties in Table 1 are most likely higher for several of the studies, when all uncertainties (including standard and decay constant uncertainties) are fully propagated according to current standards (Renne et al., 2009). Based on the current literature we can conclude that early Miocene volcanism in the northern part of the MCC and along the İBTZ is roughly constrained between ~14 and ~18 Ma with ages around ~20 Ma at some locations (Fig. 3 and Table 1). The middle to late Miocene volcanism occurred between ~7 Ma and ~14 Ma based on published geochronological data with the majority of the data between ~11 and ~14 Ma. The ages are mostly based on the K/Ar technique and some on Ar/Ar geochronology (Table 1). K/Ar data should be treated with some caution, as the method can underestimate ages due to incomplete extraction of $^{40}Ar^*$ from a sample and results do not reveal sample heterogeneities or complexities (e.g. McDougall and Harrison, 1999). The granitic intrusions yield ages between ~17 and ~23 Ma for

the Eğrigöz, Alaçamdağ and Eybek intrusions, ~11–15 Ma for the Cyclades and ~52 Ma for Orhaneli. The intrusions within the footwall of Gediz Detachment (Turgutlu and Salihli granites) are dated between 9 and 22 Ma (Fig. 2 and Table 1).

Age data compiled from the literature and radioisotope age results from this study indicate that the first magmatic activity along the İBTZ took place during the Burdigalian (Fig. 6), corroborated by the oldest $^{40}Ar/^{39}Ar$ age of ~19.7 Ma (Table 2) obtained from the Yuntdağ volcanics of the lower sequence (Figs. 5 and 6). The youngest age of the lower sequence magmatism is obtained from Çandarlı volcanics (CAN2), which yielded an $^{40}Ar/^{39}Ar$ age of ~ 16.1 Ma (Table 2), corresponding to the Burdigalian-Langhian boundary (Fig. 6). $^{40}Ar/^{39}Ar$ age results from the upper sequence indicate that the rhyolitic rocks were emplaced around 13.1 Ma, while the basaltic columnar lavas were extruded between 13.0 and 13.7 Ma (Fig. 6 and Table 2). Likewise, Borsi et al. (1972) and Göktaş et al. (2013) also reported similar ages (12.5 and 13.8 Ma) from the region, respectively. Therefore, the second stage of volcanic activity emplaced within the upper sequence deposits are dated as Serravalian (Fig. 6).

Based on extensive geochemical studies in the area (Innocenti et al., 2005; Pearce and Stern, 2006; Yılmaz and Pearce, 2007; Karacık et al., 2007; Helvacı et al., 2009; Altunkaynak et al., 2010; Ersoy et al.,
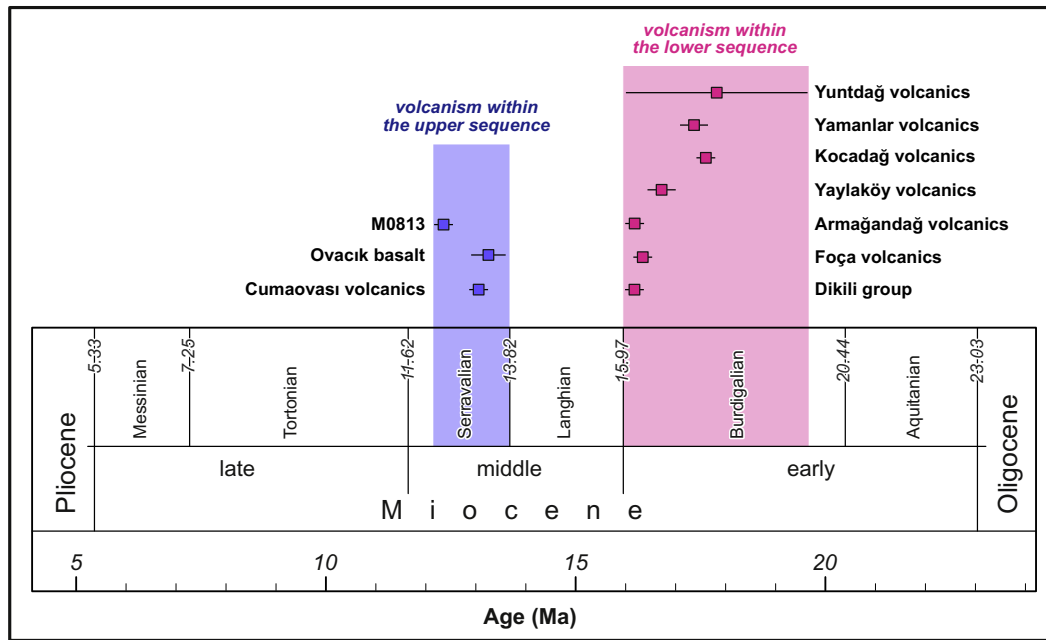
Fig. 6. Chronologic position of ^{40}Ar/^{39}Ar results and spatio-temporal relationship between volcanism and studied areas. There are two distinct age groups around 12.0–13.5 Ma and 16.0–18.0 Ma that are also is in agreement with the stratigraphic record of volcanism in lower (pink) and upper (blue) sequence of Miocene sedimentary units.

2012a; Karacık and Genç, 2013), trace element and isotopic data were correlated to our ^{40}Ar/^{39}Ar age data (Table S1). This allows interpretation of the geochemistry with respect to the two age groups of early and middle-late Miocene. The positive correlation between SiO_2 and ^{87}Sr/^{86}Sr is readily explained by crustal assimilation (Fig. 8a). However, Ersoy et al. (2012a) describe two evolutionary trends (Fig. 8a) starting from the basaltic rocks (late Miocene, Ovacık and Yağcılar) and primitive andesitic rocks (e.g., early Miocene, Yuntağı). Cumaovası volcanics and evolved rocks of Yuntağı lie on this second crustal assimilation curve. Rhyolites from the Foça volcanics follow a different trend, which can be explained with fractional crystallization (Ersoy et al., 2012a). Trachytes from the Foça volcanics (0.7075) could have also been produced solely by fractional crystallization. On the ^{87}Sr/^{86}Sr versus age diagram (Fig. 8b), different ^{87}Sr/^{86}Sr ratios show different degrees of crustal assimilation, which may be correlated to extension in the crust. It is difficult to determine whether upper or lower crust was involved in assimilation based on ^{87}Sr/^{86}Sr ratios, because lower crustal rocks (e.g. Ios Augen gneiss) have ratios of ~0.72 and upper crustal rocks (e.g. metapelite from Santorini) have ratios of 0.709–0.739 (Klaver et al., 2016). However, ^{87}Sr/^{86}Sr ratios of around 0.709 (e.g. Cumaovası volcanics) could reflect assimilation in the upper crust. Assuming the andesites of Yuntağı represent the original composition, the Yuntağı andesites and trachytes experienced more assimilation than the younger volcanism in Kocadağ, Yaylaköy, and Yuntağı (rhyolites and dacites). After the hiatus, Ovacık and Yağcılar basalts erupted, which have low ^{87}Sr/^{86}Sr ratios (0.7062–0.7075). These late Miocene basalts were possibly not affected by significant crustal assimilation and can be therefore used as an end-member. Cumaovası volcanics (dacites and rhyolites with very high ratios) show significant amounts of assimilation.

N-MORB normalized trace element abundance patterns show Ba, Nb, and Eu anomalies. Negative Ba and Nb anomalies are especially pronounced in rhyolitic samples and a mafic sample from Foca, both middle to late Miocene. The Nb anomaly from different samples is evaluated with the Th/Nb trace element ratio plotted against both SiO_2 content (Fig. 8c) and age (Fig. 8d). The Th/Nb ratio for the early Miocene group is between 1 and 2.69 (highest in Yuntağ trachyte, 18.51 Ma; excluding Yaylaköy). The middle-late Miocene group displays low ratios of <1 for samples from the young basalts (Ovacık, Yağcılar, Yarantepe) and the trachyte - phonolite rocks of Foça. The young rhyolites of Urla are

slightly higher than 1, the rhyolites of Cumovası have ratios between 0.79 and 2.62, and the dacites of Cumovasi have high ratios of >3. Compared to depleted mantle, enriched mantle (Kula, Alıcı et al., 2002), and sediment (EMS, Klaver et al., 2016), the ratios of the samples are much higher.

Ba/Nb ratios do not show a clear correlation with SiO_2 and might be prone to modification by fluid alteration (Fig. 8e). However, late Miocene Urla and Cumaovası rhyolites, the Foça trachyte and phonolite, as well as middle Miocene Foça rhyolites, have low Ba/Nb ratios, suggesting a smaller subduction component for areas without extensive assimilation (Foça, Fig. 8f). The Zr/Nb ratios suggest mixing between mantle melt and sediments (EMS). Less sediment/upper crustal imprint is observed in the Cumaovası and Foça rhyolites (Fig. 8g and h).

4.2. Implications for the Miocene basin formation in circum-western Anatolia

As discussed previously, two different sedimentary sequences are recognized within the İBTZ during the Miocene. Both of these sequences are dominated by lacustrine deposits and interlayered with volcanic rocks. Our new geochronologic data and compilation of published biostratigraphic ages (de Bruijn et al., 2006 and Kaya et al., 2007) indicate that the earliest deposition in the region commenced by the early Burdigalian (~20 Ma). This phase lasted until ~16 Ma (CAN2 from Dikili) after the emplacement of youngest volcanic rocks of the lower sequence (Figs. 3 and 6). The oldest radioisotope ages obtained from the upper sequence date the commencement of deposition of this sequence at ~13.7 Ma. This difference implies that the hiatus between the lower and upper sequences is around 2.3 Ma (Figs. 6 and 7). The youngest age obtained from the upper sequence is ~12.3 Ma, although rodent ages suggest that the deposition of the upper sequence continued until Tortonian (Kaya et al., 2007). Similarly, Tortonian ages for the upper sequence are also reported from the easternmost part of the Büyük Menderes Graben in the Denizli Basin (Kaymakci, 2006). Apart from these, Şen and Seyitoğlu (2009) claimed that there is no interruption indeposition within the Gediz and Büyük Menderes Grabens. However, İztan and Yazman (1990), Ediger et al. (1996), Yazman et al. (1998, 2000), Emre and Sözbilir (2007), Uzel et al. (2017) documented ample stratigraphic evidence for a mid-Miocene unconformity within these
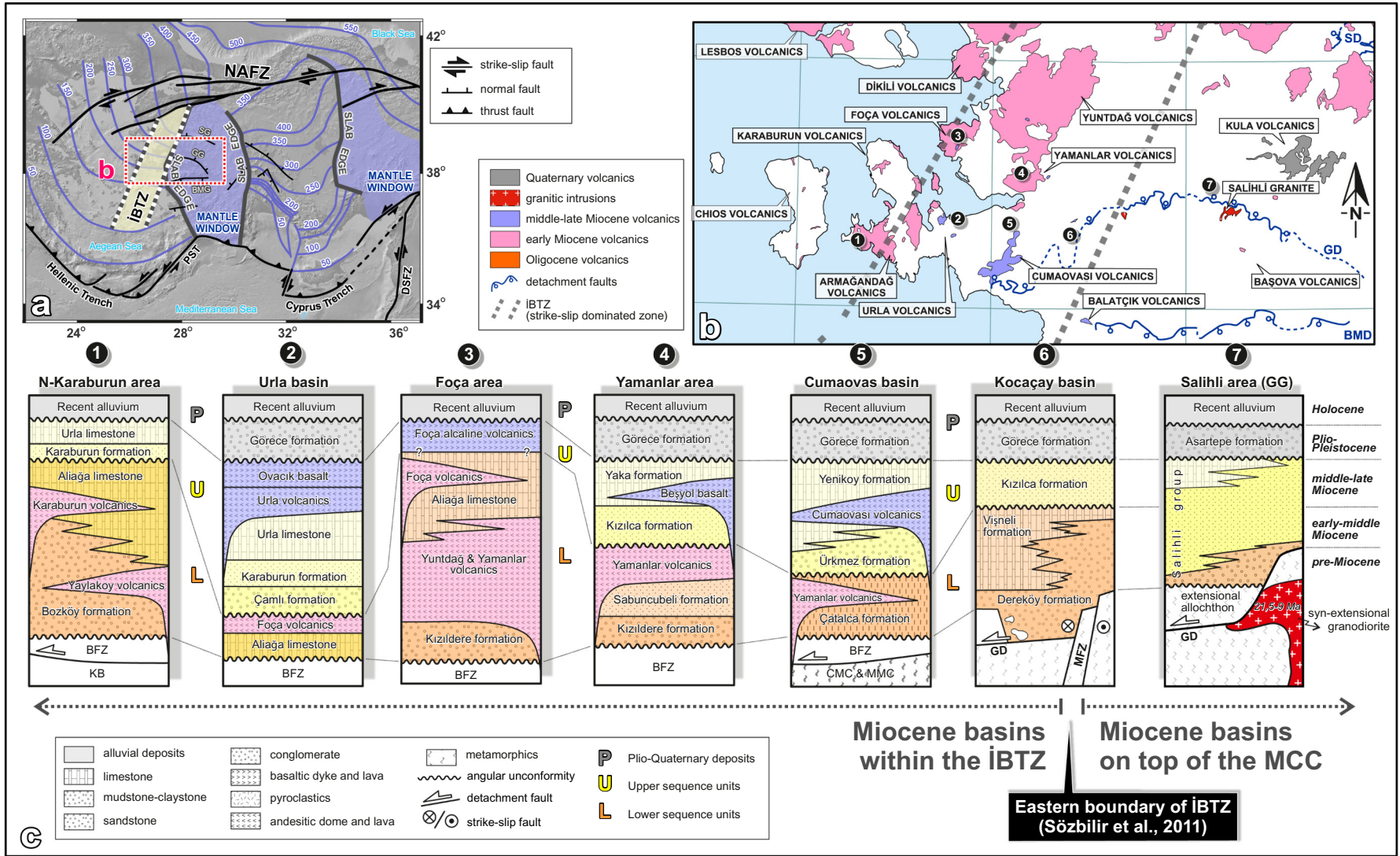
Fig. 7. a) Generalized tectonic map showing the contours (in km) of the Aegean and the Cyprean slabs with major structural elements of the area (Biryol et al., 2011). NAFZ, North Anatolian Fault Zone; PST, Pliny-Strabo Trench (STEP Fault); DSFZ, Dead Sea Fault Zone; BMG, Büyük Menderes Graben; GG, Gediz Graben; SG, Simav Graben. **b)** Simplified geological map including the distribution of Miocene magmatic rocks around the IBTZ. SD, Simav Detachment; GD, Gediz Detachment; BMD, Büyük Menderes Detachment. **c)** Vertical stratigraphic geometry of Miocene basins and their lateral correlations, west to east (modified from Kaya, 1981; Akay & Erdoğan, 2001; Helvacı et al., 2009; Uzel et al., 2012; Sözbilir et al., 2011). GD, Gediz Detachment; MFZ, Mahmutdağ Fault Zone; BFZ, Bornova Flysch Zone; KB, Karaburun Belt; CMC, Cycladic Metamorphic Core Complex; MMC, Menderes Metamorphic Core Complex; GG, Gediz Graben.

Fig. 8. SiO$_2$ and Age versus ^{87}Sr/^{86}Sr (**a, b**); Th/Nb (c,d); Ba/Nb (**d,e**) and Zr/Nb (**f, g**). The fields shown in the SiO2 versus ^{87}Sr/^{86}Sr diagram are based on Ersoy et al. (2012a). Kula is used as proxy for enriched mantle (Alici et al. 2002), Eastern Mediterranean Sediment (EMS) is used as proxy for subducted sediment (Klaver et al. 2015), metapelite from Santorini is used as proxy for upper crust (UC,) and augengneiss from Ios is used as proxy for lower crust (LC, Klaver et al., 2016) and N-MORB values are from Sun and McDonough (1989).

grabens, implying that there is an apparent temporal link between volcanic activity and basin development in the region, evidenced by contemporaneous inception ages, paucity of volcanism, and a stratigraphic hiatus between the lower and upper sedimentary sequences.

4.3. Implications for the subduction dynamics of Aegean region

Recent geological and deep geophysical studies in the western Anatolian and Aegean region reveal that slab-edge processes related to roll-back and tear in the northwards subducting African oceanic slab below Anatolia control the tectonics and magmatic activity (Pe-Piper et al., 2002; Erkül et al., 2005a, 2013; Altunkaynak et al., 2010; Karacık et al., 2013;. Mantle tomographic images (van Hinsbergen et al., 2010; Biryol et al., 2011) show that there are marked differences in the upper mantle and lithospheric characteristics between the MCC and west of it. Similarly, the geochemical characteristics of Miocene volcanic rocks in the region indicate a difference in the thickness of the lithosphere beneath the western Anatolia and under the İBTZ, which is becoming thinner from east to west (Ersoy et al., 2012a). Geochemical
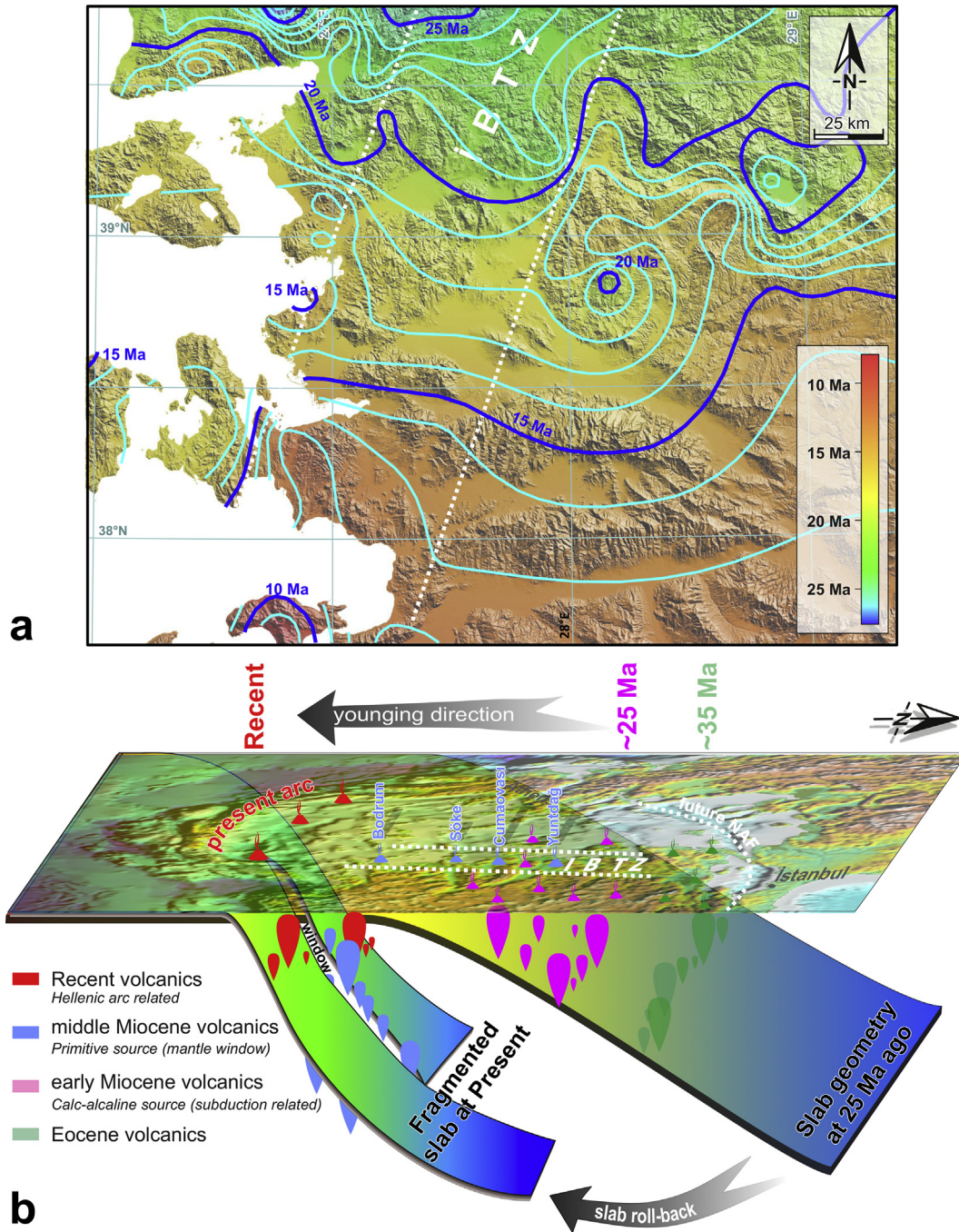
Fig. 9. a) Iso-age contour map of the Miocene volcanics in western Anatolia. The ages are compiled from the 32 $^{40}Ar/^{39}Ar$ ages of this study. The data are plotted on a Digital Elevation Model (DEM) of the area to show spatio-temporal behavior of volcanism within and around of İBTZ (ref for the DEM – is it SRTM?). **b)** Simplified surface to mantle 3D model of Aegean–west Anatolian region (modified from Faccenna et al., 2006; Biryol et al., 2011; Jolivet et al., 2013, 2015; Uzel et al., 2015) depicting the distribution of Cenozoic magmatism through the west Anatolian crust. Please note that the main possible mechanism for the southward younging of volcanics is slab roll-back. In addition, deep-seated magmatism along IBTZ is related to slab detachment and slab tear (STEP fault) processes at the northern edge of subducting African slab.

characteristics of the volcanic rocks also change from shoshonitic and ultrapotassic to high potassic affinities (Table S1) where strike-slip tectonics became dominant (Ersoy et al., 2012a). It seems that the volcanic activity in western Anatolia is always associated with the İBTZ as indicated by the positions of the eruption centers, following the trend of the İBTZ. Although the eruption centers in the lower sequence are not fully constrained to the present-day configuration of the İBTZ, the volcanic centers contemporaneous with the upper sequence are constrained within the İBTZ. Uzel et al. (2013) structurally documented that the İBTZ has evolved from a large shear zone since the early Miocene to a narrow shear zone by the Middle Miocene. There is also a distinct younging in the ages of the volcanic rocks southwards, indicating the shift of the locus of volcanism. This relationship is interpreted as the manifestation of roll-back of the subducted African Oceanic slab (Fig. 9; after Fytikas et al., 1984). These observations and results collectively imply that the İBTZ is not only accommodating differential extensional strain between the Menderes (east) and Cycladic (west) core complexes but also is a deep-seated structure developed on the overriding Eurasian plate, due to the tear along the subducting African Plate (van Hinsbergen et al., 2010; Uzel et al., 2015), and it has provided necessary permeability for the magma to reach the surface. As the İBTZ became narrower from a large shear zone in western Anatolia, it constrained the location of volcanic activity, the products of which are interlayered within the sedimentary sequences (Fig. 7). The timing of tearing is dated as Langhian with our $^{40}Ar/^{39}Ar$ data set (Fig. 6). Correlatively, a new phase of detachment faulting along the northern edge of MCC was reported by Bozkurt et al. (2011) based on Rb–Sr ages of brown and green biotite. They claimed that 18–12 Ma is a period of cessation in detachment faulting, and it resumed by 12–10 Ma associated with high angle normal faulting. Similarly, Lips et al. (2001), Hetzel et al. (2013), Buscher et al. (2013), Heineke et al. (2019) and Nilius et al. (2019) reported a distinct gap in the volcanic activity and change in the mode of deformation in the Menderes Core Complex around 15 Ma.

5. Conclusions

The thirty-five samples collected from syn-depositional volcanic rocks within the İBTZ are dated using the $^{40}Ar/^{39}Ar$ geochronology technique. Three of them yielded unreliable ages because of excess argon or alteration. The results of the remaining 32 samples, together with our field observations and data in the literature, led to the following conclusions:

- The volcanism along the İBTZ can be categorized into two main groups based on their ages and geochemical characteristics. These are: (i) early Miocene calc-alkaline and shoshonitic rocks contemporaneously emplaced and interlayered with the deposition of the lower sequence; and (ii) middle to late Miocene alkaline rocks emplaced contemporaneously and interlayered with the upper sequence.
- Early Miocene andesitic, dacitic, and basaltic andesitic lava flows, dikes, and their pyroclastics are interlayered within the lower sequence and belong to the first magmatic phase. The radio-isotope data show that this phase occurred in the Burdigalian with ages ranging between 19.66 Ma and 15.99 Ma.
- According to our new ages, a remarkable age gap in Langhian and a distinct change in geochemistry between lower and upper sequences magmatism is recognized. This gap is contemporaneous with a regional angular unconformity between the lower and upper sequences.
- The second phase of volcanism comprises mainly basaltic and rhyolitic lavas. It includes Cumaovası and Urla volcanics dated as Serravalian, ranging from 12.33 Ma and 13.69 Ma.
- The ~2.3 Ma long pause in the volcanism also corresponds to a change in the mode of extensional deformation, phases of

exhumation of the Menderes core complex, and an inversion in the rotational deformation within the İBTZ.

Supplementary data to this article can be found online at https://doi.org/10.1016/j.lithos.2019.105305.

Declaration of Competing Interest

The authors declare that they have no known competing financial interests or personal relationships that could have appeared to influence the work reported in this paper.

Acknowledgment

References

Akay, E., Erdoğan, B., 2004. Evolution of Neogene calc-alkaline to alkaline volcanism in the Aliağa–Foça region (Western Anatolia, Turkey). J. Asian Earth Sci. 24, 367–387.

Akgün, F., Olgun, E., Kuşçu, İ., Toprak, V., Göncüoğlu, M.C., 1995. New data on the stratigraphy, depositional environment, and real age of the Oligo-Miocene cover of the central Anatolian crystalline complex. TAPG Bulletin 6 (1), 51–68.

Aldanmaz, E., Pearce, J.A., Thirlwall, M.F., Mitchell, J.G., 2000. Petrogenetic evolution of Late Cenozoic, post-collision volcanism in western Anatolia, Turkey. J. Volcanol. Geotherm. Res. 102, 67–95.

Alıcı, P., Temel, A., Gourgaud, A., 2002. Pb-Nd-Sr isotope and trace element geochemistry of Quaternary extension-related alkaline volcanism: a case study of Kula region (western Anatolia, Turkey). J. Volcanol. Geotherm. Res. 115, 487–510.

Altunkaynak, Ş., Genç, Ş.C., 2008. Petrogenesis and time-progressive evolution of the Cenozoic continental volcanism in the Biga Peninsula, NWAnatolia (Turkey). Lithos 102, 316–340.

Altunkaynak, Ş., Yılmaz, Y., 1998. The Mount Kozak magmatic complex, Western Anatolia. J. Volcanol. Geotherm. Res. 85, 211–233.

Altunkaynak, Ş., Yılmaz, Y., 1999. The Kozak Pluton and its emplacement. Geol. J. 34, 257–274.

Altunkaynak, I., Rogers, N.W., Kelley, S.P., 2010. Causes and effects of geochemical variations in late Cenozoic volcanism of the Foca volcanic centre, NW Anatolia, Turkey. Int. Geol. Rev. 52, 579–607.

Altunkaynak, Ş., Dilek, Y., Genç, Ş.C., Sunal, G., Gertisser, R., Furnes, H., Foland, A.K., Yang, J., 2012. Spatial, temporal and geochemical evolution of Oligo-Miocene granitoid magmatism in western Anatolia, Turkey. Gondwana Res. 21, 961–986.

Avigad, D., Ziv, A., 2001. Ductile and brittle shortening, extension-parallel folds and maintenance of crustal thickness in the central Aegean (Cyclades, Greece). Tectonics 20 (2), 277–287.

Avigad, D., Baer, G., Heimann, A., 1998. Block rotations and continental extension in central Aegean Sea: palaeomagnetic and structural evidence from Tinos and Mykonos (Cyclades, Greece). Earth Planet. Sci. Lett. 157, 23–40.

Barka, A., 1992. The North Anatolian fault zone. Ann. Tecton. 6, 164–195.

Bellon, P.H., Jarrige, J.J., Sorel, E.D., 1979. Les activites magmatiques egeennes de l'Oligocene a nos jours et leurs cadres geodynamiques. Donnees nouvelles et synthese. Rev. Géol. Dynam. Géog. Phys. 21, 41–55.

Benda, L., Innocenti, F., Mazzuoli, R., Radicati, F., Steffens, P., 1974. Stratigraphic and radiometric data of the Neogene in Northwest Turkey (Cenozoic and Lignites in Turkey-16). Zeitschrift der Deutschen Geologischen Gesellschaft Band 125, 183–193.

Besenecker, H., 1973. Neogen und Quartär der Insel Chios (Ägäis). PhD Thesis. Freien Universität Berlin, p. 195.

Biryol, C.B., Beck, S.L., Zandt, G., Özacar, A.A., 2011. Segmented African lithosphere beneath the Anatolian region inferred from teleseismic P-wave tomography. Geophys. J. Int. 184, 1037–1057.

Bolhar, R., Ring, U., Allen, C.M., 2010. An integrated zir-con geochronological and geochemical investigation into theMiocene plutonic evolution of the Cyclades, Aegean Sea,Greece: part 1: geochronology. Contrib. Mineral. Petrol. 160, 719–742.

Borsi, J., Ferrara, G., Innocenti, F., Mazzuoli, R., 1972. Geochronology and petrology of recent volcanics in the eastern Aegean Sea (West Anatolia and Lesbos Island). Bull. Volcanol. 36, 473–496.

Bozkurt, E., 2000. Timing of extension on the Büyük Menderes Graben, western Turkey, and its tectonic implications. In: Bozkurt, E., Winchester, J.A., Piper, J.D.A. (Eds.),

Tectonics and Magmatism in Turkey and the Surrounding Area. 173. Geological Society, London, Special Publications, pp. 385–403. https://doi.org/10.1144/GSL.SP.2000.173.01.18.

Bozkurt, E., 2001. Neotectonics of Turkey—a synthesis. Geodin. Acta 14, 3–30.

Bozkurt, E., Oberhänsli, R., 2001. Menderes Massif (western Turkey): structural, metamorphic and magmatic evolution. Int. J. Earth Sci. 89, 679–882.

Bozkurt, E., Park, R.G., 1994. Southern Menderes Massif: an incipient metamorphic core complex in Western Anatolia, Turkey. J. Geol. Soc. Lond. 151, 213–216.

Bozkurt, E., Sözbilir, H., 2004. Tectonic evolution of the Gediz Graben: field evidence for an episodic two extensions in western Turkey. Geol. Mag. 141, 63–79.

Bozkurt, E., Sözbilir, H., 2006. Evolution of the largescale active Manisa fault, southwest Turkey: Implications on fault development and regional tectonics. Geodin. Acta 19 (6), 427–453. https://doi.org/10.3166/ga.19.427-453.

Bozkurt, E., Winchester, J.A., Ruffet, G., Rojay, B., 2009. Age and chemistry of miocene volcanic rocks from the kiraz basin of the Küçük Menderes Graben: its significance for the extensional tectonics of Southwestern Anatolia, Turkey. Geodin. Acta 21, 239–257.

Bozkurt, E., Satır, M., Buğdaycıoğlu, Ç., 2011. Surprisingly young Rb/Sr ages from the Simav extensional detachment fault zone, northern Menderes Massif, Turkey. J. Geodyn. 52 (5), 406–431.

Boztuğ, D., Harlavan, Y., Jonckheere, R., Can, I., Sarı, R., 2009. Geochemistry and K–Ar cooling ages of the Ilıca, Cataldag (Balıkesir) and Kozak (Izmir) granitoids, west Anatolia, Turkey. Geological Journal 44, 79–103.

Brichau, S., Ring, U., Carter, A., Monié, P., Bolhar, R., Stockli, D.F., Brunel, M., 2007. Extensional faulting on Tinos Island, Aegean Sea, Greece: how many detachments. Tectonics 26, TC4009. https://doi.org/10.1029/2006TC001969.

Buscher, J.T., Hampel, A., Hetzel, R., Dunkl, I., Glotzbach, C., Struffert, A., Akal, C., Rätz, M., 2013. Quantifying rates of detachment faulting and erosion in the central Menderes Massif (western Turkey) by thermochronology and cosmogenic 10Be. J. Geol. Soc. 170 (4), 669–683.

Candan, O., Dora, O.Ö., Oberhansli, R., Çetinkaplan, M., Partzsch, J.H., Warkus, F.C., Dürr, S., 2001. Pan-African high-pressure metamorphism in the Precambrian basement of the Menderes Massif, Western Anatolia, Turkey. Int. J. Earth Sci. 89, 793–811.

Catlos, E.J., Baker, C., Sorensen, S.S., emen, C,., Hancer, M., 2010. Geochemistry, geochronology, and cathodoluminescence imagery of the Salihli and Turgutlu granites (central Menderes Massif, western Turkey): implications for Aegean tectonics. Tectonophysics 48, 110–130.

Çiftçi, N.B., Bozkurt, E., 2009. Evolution of the Miocene sedimentary fill of the Gediz graben, SW Turkey. Sediment. Geol. 216 (3–4), 49–79. https://doi.org/10.1016/j.sedgeo.2009.01.004.

Çiftçi, N.B., Bozkurt, E., 2010. Structural evolution of the Gediz Graben, SW Turkey: temporal and spatial variation of the graben basin. Basin Res. 22, 846–873.

de Bruijn, H., Mayda, S., van den Hoek Ostende, L., Kaya, T., Saraç, G., 2006. Small mammals from the Early Miocene of Sabuncubeli (Manisa, S.W. Anatolia, Turkey). Beitr. Paläontol. 30, 57–87.

De Leeuw, A., Mandic, O., Vranjkovic, A., Pavelic, D., Harzhauser, M., Krijgsman, W., Kuiper, K.F., 2010. Chronology and integrated stratigraphy of the Miocene Sinj Basin (Dinaride Lake System, Croatia). Palaeogeogr. Palaeoclimatol. Palaeoecol. 292, 155–167.

Delaloye, M., Bingöl, E., 2000. Granitoids from western and northwestern Anatolia: geochemistry and modeling of geodynamic evolution. Int. Geol. Rev. 42, 241–268.

Denèle, Y., Lecomte, E., Jolivet, L., Lacombe, O., Labrousse, L., Huet, B., Le Pourhiet, L., 2011. Granite intrusion in a metamorphic core complex: the example of the Mykonos laccolith (Cyclades, Greece). Tectonophysics 501 (1–4), 52–70.

Dewey, J.F., Şengör, A.M.C., 1979. Aegean and surrounding regions, complex multiplate and continuum tectonics in a convergent zone. Bull. Geol. Soc. America Part 1 (90), 84–92.

Ediger, V., Batı, Z., Yazman, M., 1996. Paleopalynology of possible hydrocarbon source rocks of the Alaşehir–Turgutlu area in the Gediz graben (western Anatolia). Turkish Assoc. Petrol. Geol. Bull. 8, 94–112.

Emre, T., 1996. Geology and tectonics of the Gediz Graben. Turk. J. Earth Sci. 5, 171–185.

Emre, T., Sözbilir, H., 2005. Geology, geochemistry and geochronology of the Başlova andesite, eastern end of the Küçük Menderes Graben. Bull. Min. Res. Exp. 131, 1–19.

Emre, T., Sözbilir, H., 2007. Tectonic evolution of the KirazBasin, Küçük Menderes Graben: Evidence for compres-sion/uplift-related basin formation overprinted by extensional tectonics in Western Anatolia. Turkish J. Earth Sci. 16, 441–470.

Emre, Ö., Özalp, S., Duman, T.Y., 2011. 1:250.000 ölçekli Türkiye diri fay haritası serisi, İzmir (NJ35–7) Paftası, Seri No: 6. Maden Tetkik ve Arama Genel Müdürlüğü, Ankara-Türkiye.

Ercan, T., Satır, M., Kreuzer, M., Türkecan, H., Günay, A., Çevikbaş, E., Ateş, A., Can, M., 1985. Batı Anadolu Senozoyik volkanitlerine ait yeni kimyasal, izotopik ve radyometrik verilerin yorumu (Interpretation of the new geochemical, isotopic and radiometric age data from the western Anatolia Cenozoic volcanics). Bulletin of the Geological Society of Turkey 28, 121–136.

Ercan, T., Satır, M., Steinitz, G., Dora, A., Sarıfakıoğlu, E., Adis, C., Walter, H.J., Yıldırım, T., 1995. Biga Yarımadası ile Gökçeada, Bozcaada ve Tavsan adalarındaki (KB Anadolu) Tersiyer volkanizmasının özellikleri. MTA Dergisi 117, 55–86.

Ercan, E., Satır, M., Sevin, D., Türkecan, A., 1996. Some new radiometric ages from Tertiary and Quaternary volcanic rocks from West Anatolia. Bull. Min. Res. Exp. 119, 103–112.

Erkül, F., Helvacı, C., Sözbilir, H., 2005a. Evidence for two episodes of volcanismin the Bigadic borate basin and tectonic implications for western Turkey. Geol. J. 40, 545–570.

Erkül, F., Helvacı, C., Sözbilir, H., 2005b. Stratigraphy and geochronology of the Early Miocene volcanic units in the Bigadiç Borate Basin, Western Turkey. Turk. J. Earth Sci. 14, 227–253.

Erkül, F., 2010. Tectonic significance of synextensional ductile shear zones within the Early Miocene Alaçamdağ granites, northwestern Turkey. Geol. Mag. 147, 611–637.

Erkül, F., Erkül, S.T., Ersoy, Y., Uysal, İ., Klötzli, U., 2013. Petrology, mineral chemistry and Sr–Nd–Pb isotopic compositions of granitoids in the central Menderes metamorphic core complex: constraints on the evolution of Aegean lithosphere slab. Lithos 180, 74–91.

Ersoy, Y., Helvacı, C., Sözbilir, H., Erkül, F., Bozkurt, E., 2008. A geochemical approach to Neogene–Quaternary volcanic activity of western Anatolia: an example of episodic bimodal volcanism within the Selendi Basin, Turkey. Chem. Geol. 255, 265–282.

Ersoy, Y.E., Helvacı, C., Uysal, İ., Karaoğlu, Ö., Palmer, M.R., Dindi, F., 2012a. Petrogenesis of the Miocene volcanism along the İzmir-Balıkesir Transfer Zone in western Anatolia, Turkey: Implications for origin and evolution of potassic volcanism in post-collisional areas. J. Volcanol. Geotherm. Res. 241, 21–38.

Ersoy, Y., Dindi, F., Karaoğlu, Ö., Helvacı, C., 2012b. Soma Havzası ve Çevresindeki Miyosen Volkanizmasının Petrografik ve Jeokimyasal Özellikleri. Yerbilimleri 33, 59–80.

Ersoy, E.Y., Çemen, İ., Helvacı, C., Billor, Z., 2014. Tectono-stratigraphy of the Neogene basins in Western Turkey: Implications for tectonic evolution of the Aegean Extended Region. Tectonophysics 635, 33–58.

Faccenna, C., Bellier, O., Martinod, J., Piromallo, C., Regard, V., 2006. Slab detachment beneath eastern Anatolia: a possible cause for the formation of the North Anatolian fault. Earth Planet. Sci. Lett. 242, 85–97.

Fytikas, M., Innocenti, F., Manetti, P., Peccerillo, A., Mazzuoli, R., Villari, L., 1984. Tertiary to Quaternary evolution of volcanism in the Aegean region. Geol. Soc. Lond., Spec. Publ. 17 (1), 687–699.

Genç, S.C., Altunkaynak, Ş., Karacık, Z., Yılmaz, Y., 2001. The Çubukludağ graben, Karaburun peninsula: it's tectonic significance in the Neogene geological evolution of the western Anatolia. Geodin. Acta 14, 45–55.

Gessner, K., Piazolo, S., Güngör, T., Ring, U., Kroner, A., Passchier, C.W., 2001. Tectonic significance of deformation patterns in granitoid rocks of the Menderes nappes, Anatolide belt, southwest Turkey. Int. J. Earth Sci. 89, 766–780.

Gessner, K., Gallardo, L.A., Markwitz, V., Ring, U., Thomson, S.N., 2013. What caused the denudation of the Menderes Massif: Review of crustal evolution, lithosphere structure, and dynamic topography in southwest Turkey. Gondwana Res. 24 (1), 243–274.

Glodny, J., Hetzel, R., 2007. Precise U-Pb ages of syn-extensional Miocene intrusions in the central Menderes Massif, western Turkey. Geol. Mag. 144, 235–246.

Göktaş, A., Mutlu, I.H., Yamada, Y., 2013. Influence of Fe-doping on the structural, optical, and magnetic properties of ZnO thin films prepared by sol–gel method. Superlattice. Microst. 57, 139–149.

Gradstein, F., Ogg, J., Schmitz, M., Ogg, G., 2012. The Geologic Time Scale. Elsevier, pp. 1–1176.

Harris, N.B.W., Kelley, S., Okay, A.I., 1994. Post-collisional magmatism and tectonics in northwest Anatolia. Contrib. Mineral. Petrol. 117, 241–252.

Hasözbek, A., Akay, E., Erdoğan, B., Satır, M., Siebel, W., 2010. Early Miocene granite formation by detachment tectonics or not? A case study from the northern Menderes Massif (Western Turkey). Journal of Geodynamics 50, 67–80.

Hasözbek, A., Satır, M., Erdoğan, B., Akay, E., Sıebel, W., 2011. Early Miocene post-collisional magmatism in NW Turkey: geochemical and geochronological constraints. Int. Geol. Rev. 53, 1098–1119.

Heineke, C., Hetzel, R., Nilius, N.P., Zwingmann, H., Todd, A., Mulch, A., Wölfler, A., Glotzbach, C., Akal, C., Dunkl, I., Raven, M., 2019. Detachment faulting in a bivergent core complex constrained by fault gouge dating and low-temperature thermochronology. J. Struct. Geol. 127, 103865.

Helvacı, C., Alonso, R.N., 2000. Borate deposits of Turkey and Argentina; a summary and geological comparison. Turk. J. Earth Sci. 24, 1–27.

Helvacı, C., Ersoy, Y., Sözbilir, H., Erkül, F., Sümer, Ö., Uzel, B., 2009. Geochemistry and 40Ar/39Ar geochronology of Miocene volcanic rocks from the Karaburun Peninsula: implications for amphibole-bearing lithospheric mantle source, Western Anatolia. J. Volcanol. Geotherm. Res. 185, 181–202.

Hetzel, R., Ring, U., Akal, C., Troesch, M., 1995. Miocene NNE-directed extensional unroofing in the Menderes Massif, southwestern Turkey. J. Geol. Soc. Lond. 152, 639–654.

Hetzel, R., Zwingmann, H., Mulch, A., Gessner, K., Akal, C., Hampel, A., Güngör, T., Petschick, R., Mikes, T., Wedin, F., 2013. Spatiotemporal evolution of brittle normal faulting and fluid infiltration in detachment fault systems: A case study from the Menderes Massif, western Turkey. Tectonics 32 (3), 364–376.

Hüsing, S.K., Kuiper, K.F., Link, W., Hilgen, F.J., Krijgsman, W., 2009. The upper Tortonian - lower Messinian at Monte dei Corvi (Northern Apennines, Italy): Completing a Mediterranean reference section for the Tortonian Stage. Earth Planet. Sci. Lett. 282, 140–157.

Innocenti, F., Agostini, S., Di Vincenzo, G., Doglioni, C., Manetti, P., Savaşçın, M.Y., Tonarini, S., 2005. Neogene and Quaternary volcanism inWestern Anatolia: magma sources and geodynamic evolution. Mar. Geol. 221, 397–421.

Işık, V., Tekeli, O., 2001. Late orogenic crustal extension in the northern Menderes massif (western Turkey): evidence for metamorphic core complex formation. Int. J. Earth Sci. 89, 757–765.

Işık, V., Seyitoğlu, G., Çemen, İ., 2003. Ductile–brittle transition along the Alaşehir detachment fault and its structural relationship with the Simav detachment fault, Menderes Massif, western Turkey. Tectonophysics 374, 1–18.

Işık, V., Tekeli, O., Seyitoğlu, G., 2004. The Ar-40/Ar-39 age of extensional ductile deformation and granitoid intrusion in the northern Menderes core complex: implications for the initiation of extensional tectonics in Western Turkey. J. Asian Earth Sci. 23, 555–566.

İztan, H., Yazman, M., 1990. Geology and hydrocarbon potential of the Alaşehir (Manisa) area, western Turkey. In: Savaşçın, M.Y., Eronat, A.H. (Eds.), Proceedings of International Earth Sciences Congress on Aegean Regions, İzmir. 1, pp. 327–338.

Jolivet, L., Menant, A., Sternai, P., Rabillard, A., Arbaret, L., 2015. The geological signature of a slab tear below the Aegean. Tectonophysics, Elsevier 659, 166–182.

Karacık, Z., Genç, Ş.C., 2013. Volcano-stratigraphy of the extension-related silicic volca-nism of the Çubukludağ Graben, western Turkey: An example of generation of pyro-clastic density currents. Geol. Mag. 151, 492–516.

Karacık, Z., Yılmaz, Y., 1998. Geology of the ignimbrites and the associated volcano–plutonic complex of the Ezine area, northwestern Anatolia. J. Volcanol. Geotherm. Res. 85, 251–264.

Karaoğlu, Ö., Helvacı, C., Ersoy, E.Y., 2010. Petrogenesis and ^{40}Ar/^{39}Ar geo-chronology of the volcanic rocks of the Uşak–Güre basin, western Turkey. Lithos 119, 193–210.

Kaya, O., 1981. Miocene reference section for the coastal parts of West Anatolia. Newsl. Stratigr. 10, 164–191.

Kaya, O., Ünay, G., Eichhorn, S., Hassenrück, S., Knappe, A., Pekdeğer, A., 2004. Halitpaşa Transpressive Zone: Implications for an Early Pliocene compressional phase in central western Anatolia, Turkey. Turk. J. Earth Sci. 13, 1–13.

Kaya, O., Ünay, E., Göktaş, F., Saraç, G., 2007. Early Miocene stratigraphy of Central West Anatolia, Turkey: implications for the tectonic evolution of the Eastern Aegean area. Geol. J. 42, 85–109.

Kaymakci, N., 2006. Kinematic development and paleostress analysis of Denizli Basin (W Turkey): implications of spatial variation of relative paleostress magnitudes and ori-entations. J. Asian Earth Sci. 27, 207–222.

Kaymakci, N., Aldanmaz, E., Langereis, C., Spell, T.L., Gurer, O.F., Zanetti, K.A., 2007. Late Miocene transcurrent tectonics in NW Turkey: evidence from palaeomagnetism and 40Ar–39Ar dating of alkaline volcanic rocks. Geological Magazine 144 (2), 379–392.

Keay, S., Lister, G., Buick, I., 2001. The timing of partial melting, Barrovian metamorphism and granite intrusion in the Naxos metamorphic core complex, Cyclades, Aegean Sea, Greece. Tectonophysics 342, 275–312.

Kissel, C., Laj, C., Şengör, A.M.C., Poisson, A., 1987. Paleomagnetic evidence for rotation in opposite senses of adjacent blocks in Northeastern Aegea and western Anatolia. Geophys. Res. Lett. 14, 907–910.

Klaver, M., Carey, S., Nomikou, P., Smet, I., Godelitsas, A., Vroon, P., 2016. A distinct source and differentiation history for Kolumbo submarine volcano, Santorini volcanic field, Aegean arc. Geochem. Geophys. Geosyst. 17, 3254–3273.

Koçyiğit, A., Özaçar, A.A., 2003. Extensional neotectonic regime through the NE edge of the Outer Isparta Angle, SW Turkey: new field and seismic data. Turk. J. Earth Sci. 12, 67–90.

Koçyiğit, A., Yusufoğlu, H., Bozkurt, E., 1999. Evidence from the Gediz graben for episodic two-stage extension in western Turkey. J. Geol. Soc. Lond. 156, 605–616.

Kokkalas, S., Aydın, A., 2013. Is there a link between faulting and magmatism in the south-central Aegean Sea? Geol. Mag. 150, 193–224.

Koppers, A.A.P., 2002. ArArCALC-software for 40Ar/39Ar age calculations. Comput. Geosci. 28, 605–619.

Krijgsman, W., Hilgen, F.J., Raffi, I., Sierro, F.J., Wilson, D.S., 1999. Chronology, causes and progression of the Messinian salinity crisis. Nature 400 (6745), 652.

Krushensky, R.D., 1976. Neogene calc-alkaline extrusive rocks of the Karalar–Yesiller area, northwest Anatolia, Turkey. Bull. Volcanol. 40, 336–360.

Kuiper, K.F., Hilgen, F.J., Steenbrink, J., Wijbrans, J.R., 2004. 40Ar/39Ar ages of tephras in-tercalated in astronomical tuned Neogene sedimentary sequences in the eastern Mediterranean. Earth and Planetary. Sci. Lett. 222, 583–597.

Kuiper, K.F., Deino, A., Hilgen, F.J., Krijgsman, W., Renne, P.R., Wijbrans, J.R., 2008. Syn-chronizing rock clocks of Earth history. Science 320, 500–504.

Le Pichon, X., Angelier, J., 1979. The Hellenic arc and trench system: A key to the neotectonic evolution of the eastern Mediterranean area. Tectonophysics 60, 1–42.

Lefebvre, G.H., Hozalski, R., Novak, P.J., 2012. The role of biodegradation in limiting the ac-cumulation of petroleum hydrocarbons in raingarden soils. Water Res. 46 (20). https://doi.org/10.1016/j.watres.2011.12.040.

Lips, A.L.W., Cassard, D., Sözbilir, H., Yılmaz, H., Wijbrans, J.R., 2001. Multistage exhuma-tion of the Menderes Massif, western Anatolia (Turkey). Int. J. Earth Sci. 89, 781–792.

McDougall, I., Harrison, T.M., 1999. Geochronology and Thermochronology by the ^{40}Ar/^{39}Ar Method. Oxford University Press on Demand, Oxford.

Meulenkamp, J.E., Wortel, M.J.R., van Wamel, W.A., Spakman, W., Hoogerduyn, S.E., 1988. On the Hellenic subduction zone and the geodynamical evolution of Crete since the late middle Miocene. Tectonophysics 146, 203–215.

Min, K., Mundil, R., Renne, P.R., Ludwig, K.R., 2000. A test for systematic errors in ^{40}Ar/^{39}Ar geochronology through comparison with U/Pb analysis of a 1.1-Ga rhyolite. Geochim. Cosmochim. Acta 64, 73–98.

Morris, A., Anderson, A., 1996. First paleomagnetic results from the Cyclaic Massif, Greece and their implications for Miocene extension directions and tectonic models in the Aegean. Earth Planet. Sci. Lett. 142, 397–408.

MTA, 2002. Geological Map of Turkey, scale 1:500.000.

Nier, A.O., 1950. A redetermination of the relative abundances of the isotopes of carbon, nitrogen, oxygen, argon, and potassium. Phys. Rev. 77, 789–793.

Ocakoğlu, N., Demirbağ, E., Kuşçu, İ., 2004. Neotectonic structures in the area offshore of Alaçatı, Doğanbey and Kuşadası (western Turkey): evidence of strike-slip faulting in the Aegean extensional province. Tectonophysics 391, 67–83.

Ocakoğlu, N., Demirbağ, E., Kuşçu, İ., 2005. Neotectonic structures in İzmir Gulf and sur-rounding regions (western Turkey): Evidences of strike-slip faulting with compres-sion in the Aegean extensional regime. Mar. Geol. 219, 155–171.

Okay, A.I., Tüysüz, O., 1999. Tethyan sutures of northern Turkey. Geological Society, London, Special Publications. 156, pp. 475–515.

Özkaymak, Ç., Sözbilir, H., Uzel, B., 2013. Neogene–Quaternary evolution of the Manisa Basin: Evidence for variation in the stress pattern of the İzmir-Balıkesir Transfer Zone, western Anatolia. J. Geodyn. 65, 117–135.

Pearce, J., Stern, B., 2006. Origin of back-arc basin magmas: trace element and isotope per-spectives. Geophysical Monograph Series 166, 63–86.

Pe-Piper, G., Piper, D.J.W., Kotopouli, C.N., Panagos, A.G., 1995. Neogene volcanoes of Chios, Greece: the relative importance of subduction and back-arc extension. Geolog-ical Society of London (Special Publications) 81, 213–232.

Pe-Piper, G., Piper, D.J.W., Matarangas, D., 2002. Regional implications of geochem-istry and style of emplacement of Miocene I-type diorite and granite, Delos, Cyclades, Greece. Lithos 60, 47–66.

Pe-Piper, G., Piper, D.J.W., 2007. Neogene back-arc volcanism of the Aegean: New insights into the relationship between magmatism and tectonics. In: Beccaluva, L., et al., (eds.), Cenozoic volcanism in the Mediterranean area. Geological Society of America Special Paper 418, 17–31.

Philippon, M., Brun, J.P., Gueydan, F., Sokoutis, D., 2014. The interaction between Aegean back-arc extension and Anatolia escape since Middle Miocene. Tectonophysics 631, 176–188.

Pişkin, Ö., 1980. Kadıkalesi-Girelbelen (Bodrum yarımadası) hidrotermal ve kontakt metasomatik Pb, Zn, Cu cevherleşmelerinin mineralojik ve jeolojik incelenmesi. The-sis. Ege University, Izmir.

Purvis, M., Robertson, A., Pringle, M., 2005. Ar^{40}-Ar^{39} dating of biotite and sanidine in tuff-aceous sediments and related intrusive rocks: implications for the Early Miocene evo-lution of the Gördes and Selendi basins, W Turkey. Geodinamica Acta 18 (3-4), 239–253.

Renne, P.R., Swisher, C.C., Deino, A.L., Karner, D.B., Owens, T.L., DePaolo, D.J., 1998. Inter-calibration of standards, absolute ages and uncertainties in ^{40}Ar/^{39}Ar dating. Chem. Geol. 145, 117–152.

Renne, P.R., Deino, A.L., Hames, W.E., Heizler, M.T., Hemming, S.R., Hodges, K.V., Koppers, A.A., Mark, D.F., Morgan, L.E., Phillips, D., Singer, B.S., 2009. Data reporting norms for 40Ar/39Ar geochronology. Quat. Geochronol. 4 (5), 346–352.

Ring, U., Collins, A.S., 2005. U-Pb SIMS dating of synkinematic granites: timing of core complex formation in the northern Anatolide belt of western Turkey. J. Geol. Soc. 162, 1–10.

Ring, U., Susanne, L., Matthias, B., 1999. Structural analysis of a complex nappe sequence and late orogenic basins from the Aegean Island of Samos, Greece. J. Struct. Geol. 21, 1575–1601.

Ring, U., Wıllner, A., Lackmann, W., 2001. Stacking of nappes with different pressure-temperature paths: an example from the Menderes nappes of western Turkey. Am. J. Sci. 301, 912–944.

Ring, U., Johnson, C., Hetzel, R., Gessner, K., 2003. Tectonic denudation of a Late Cretaceous–Tertiary collisional belt: Regionally symmetric cooling patterns and their relation to extensional faults in the Anatolide belt of western Turkey. Geol. Mag. 140, 421–441.

Robert, U., Cantagrel, J.M., 1977. Le volcanisme basaltique dans le sud-est de la mer Egee; Donnees geochronologiques et relations avec la tectonique: VI. Colloquium on the Geology of the Aegan Region.

Şan, O., 1998. Geology of the Basement and Tertiary Cover Rocks of Menderes Massif in the South of Ahmetli (Manisa). MSc thesis. Ankara University.

Sarıca, N., 2000. The Plio-Pleistocene age of Büyük Menderes and Gediz Grabens and their tectonic significance on N–S extensional tectonics in West Anatolia: mammalian ev-idence from the continental deposits. Geol. J. 35, 1–24.

Schneider, C., Leung, E., Brown, J., Tollervey, D., 2009. The N-terminal PIN domain of the exosome subunit Rrp44 harbors endonuclease activity and tethers Rrp44 to the yeast core exosome. Nucleic Acids Res. 37, 1127–1140.

Şen, S., Seyitoğlu, G., 2009. Magnetostratigraphy of early–middle Miocene deposits from east–west trending Alasehir and Büyük Menderes grabens in, western Turkey, and its tectonic implications. In: van Hinsbergen, D.J.J., Edwards, M.A., Govers, R. (Eds.), Collision and Collapse at the Africa– Arabia–Eurasia Subduction Zone. 311. Geological Society, London, Special Publications, pp. 321–342.

Şengör, A.M.C., 1987. Cross-faults and differential stretchingof hanging walls in regions of low angle normal faulting: Examples from western Turkey. In ContinentalExtensional Tectonics, Eds: Coward, M.P., Dewey J.F., Hancock P.L. Geol. Soc. Spec. Publ. 28, 575–589.

Şengör, A.M.C., Yılmaz, Y., 1981. Tethyan evolution of Turkey: a plate tectonic approach. Tectonophysics 75, 181–241.

Şengör, A.M.C., Görür, N., Şaroğlu, F., 1985. Strike-slip faulting and related basin formation in zones of tectonic escape: Turkey as a case study. In: Biddle, K., Christie-Blick, N. (Eds.), Strike-Slip Deformation, Basin Formation and Sedimentation. 37. Society of Economic Paleontologists and Mineralogists, Special Publications, pp. 227–264.

Seyitoğlu, G., Scott, B.C., 1996. The cause of N–S extensional tectonics in western Turkey: tectonic escape vs back-arc spreading vs orogenic collapse. J. Geodyn. 22, 145–153.

Seyitoğlu, G., Benda, L., Scott, B.C., 1994. Neogene palynological and isotopic age data from Görde Basin, West Turkey. Newsl. Stratigr. 31, 133–142.

Seyitoğlu, G., Anderson, D., Nowell, G., Scott, B.C., 1997. The evolution from Miocene po-tassic to Quaternary sodic magmatism in western Turkey: implications for enrich-ment processes in the lithospheric mantle. J. Volcanol. Geotherm. Res. 76, 127–147.

Sözbilir, H., 2001. Extensional tectonics and the geometry of related macroscopic struc-tures: field evidence from the Gediz detachment, western Turkey. Turk. J. Earth Sci. 10, 51–67.

Sözbilir, H., 2002. Geometry and origin of folding in the Neogene sediments of the Gediz Graben, western Anatolia, Turkey. Geodin. Acta 15, 277–288.

Sözbilir, H., 2005. Oligo-Miocene extension in the Lycian orogen: evidence from the Ly-cian molasse basin. SW Turkey. Geodinamica Acta 18, 257–284.

Sözbilir, H., Emre, T., 2011. Supradetachment Basin and rift Basin Developed During the Neotectonic Evolution of the Menderes Massif. Geological Congress of Turkey, Ankara, pp. 300–301 Abstracts.

Sözbilir, H., Sarı, B., Uzel, B., Sümer, Ö., Akkiraz, S., 2011. Tectonic implications of transtensional supradetachment basin development in an extension-parallel transfer zone: the Kocaçay Basin, western Anatolia, Turkey. Basin Res. 23, 423–448.

Sümer, Ö., Inci, U., Sözbilir, H., 2013. Tectonic evolution of the Söke Basin:˙ Extension-dominated transtensional basin formation in western part of the Büyük Menderes Graben, Western Anatolia, Turkey. J. Geodyn. 65, 148–175.

Sun, S.S., McDonough, W.F., 1989. Chemical and isotopic systematics of ocean basalts: Implications for mantle composition and processes, in Magmatism in the Ocean Basins. Geol. Soc. Lond. Spec. Publ. 423, 13–345.

Tirel, C., Gautier, P., van Hinsbergen, D.J.J., Wortel, M.J.R., 2009. Sequential development of metamorphic core complexes: numerical simulations and comparison to the Cyclades, Greece. In: van Hinsbergen, D.J.J., Edwards, M.A., Govers, R. (Eds.), Collision and Collapse at the Africa–Arabia–Eurasia Subduction Zone. 311. Geological Society, London, Special Publications, pp. 257–292.

Ünay, E., Göktas, F., 1999. Söke Çevresi (Aydın) Geç-Erken Miyosen ve Kuvaterner yaşlı küçük memelileri: Ön sonuçlar. Geological Bulletin of Turkey 42, 99–113.

Ünay, E., Göktaş, F., Hakyemez, H.Y., Avşar, M., Şan, Ö., 1995. Büyük Menderes Grabeni'nin kuzey kenarındaki çökellerin Arvicolidae (Rodentia, Mammalia) faunasına dayalı olarak yaşlandırılması. Geological Bulletin of Turkey 38, 75–80.

Uzel, B., Sözbilir, H., 2008. A First record of strike-slip basin in western Anatolia and its tectonic implication: the Cumaovası basin as an example. Turk. J. Earth Sci. 17, 559–591.

Uzel, B., Sözbilir, H., Özkaymak, Ç., 2012. Neotectonic evolution of an actively growing superimposed basin in western Anatolia: The inner bay of İzmir, Turkey. Turk. J. Earth Sci. 22 (4), 439–471. https://doi.org/10.3906/yer-0910-11.

Uzel, B., Sözbilir, H., Özkaymak, Ç., Kaymakçı, N., Langereis, C.G., 2013. Structural evidence for strike-slip deformation in the İzmir-Balıkesir Transfer Zone and consequences for late Cenozoic evolution of western Anatolia (Turkey). J. Geodyn. 65, 94–116. https://doi.org/10.1016/j.jog.2012.06.009.

Uzel, B., Langereis, C.G., Kaymakci, N., Sözbilir, H., Özkaymak, Ç., Özkaptan, M., 2015. Paleomagnetic evidence for an inverse rotation history of Western Anatolia during the exhumation of Menderes core complex. Earth Planet. Sci. Lett. 414, 108–125. https://doi.org/10.1016/j.epsl.2015.01.008.

Uzel, B., Sümer, Ö., Özkaptan, M., Özkaymak, Ç., Sözbilir, H., Kaymakci, N., İnci, U., Langereis, C.G., 2017. Palaeomagnetic and geochronological evidence for a major middle Miocene unconformity in Söke Basin (western Anatolia) and its tectonic implications for the Aegean region. J. Geol. Soc. 174 (4), 721–740.

van Hinsbergen, D.J.J., 2010. A key extensional metamorphic core complex reviewed and restored: the Menderes Massif of western Turkey. Earth Sci. Rev. 102, 60–76.

van Hinsbergen, D.J.J., Hafkenscheid, E., Spakman, W., Meulenkamp, J.E., Wortel, R., 2005. Nappe stacking resulting from subduction of oceanic and continental lithosphere below Greece. Geology 33, 325–328.

van Hinsbergen, D.J., Kaymakci, N., Spakman, W., Torsvik, T.H., 2010. Reconciling the geological history of western Turkey with plate circuits and mantle tomography. Earth Planet. Sci. Lett. 297 (3-4), 674–686.

Walcott, C.R., White, S.H., 1998. Constraints on the kinematics of postorogenic extension imposed by stretching lineations in the Aegean region. Tectonophysics 298, 155–175.

Westaway, R., 1994. Present-day kinematics of the Middle East and the Eastern Mediterranean. J. Geophys. Res. 99, 12071–12090.

Westaway, R., Pringle, M., Yurtmen, S., Demir, T., Bridgland, D., Rowbotham, G., Maddy, D., 2004. Pliocene and Quaternary regional uplift in western Turkey: the Gediz river terrace staircase and the volcanism at Kula. Tectonophysics 391, 121–169.

Wijbrans, J.R., Pringle, M.S., Koppers, A.A.P., Scheveers, R., 1995. Argon geochronology of small samples using the Vulkaan argon laser probe. Proc. Kon. Nederland. Akad Weten. 98, 185–218.

Williamson, K., 1982. Geothermal prospection of the Western Anatolia Report. Union Oil Company of California, Santa Rosa-California-USA.

Yazman, M.K., Güven, A., Ermiş, Y., Yılmaz, M., Özdemir, İ, Akçay, Y., Gönülalan, U., Tekeli, Ö., Aydemir, V., Sayılıö, A., Batı, Z., İztan, H., Korucu, Ö., Grunnaleite, İ, 1998. Alaşehir grabeni ve Alaşlehir-1 prospektinin değerlendirme raporu. TPAO Report 3864 146 p.

Yılmaz, Y., 1989. An approach to the origin of young volcanic rocks of Western Turkey. In: Şengör, A.M.C. (Ed.), Tectonic Evolution of the Tethyan Region, pp. 159–189.

Yılmaz, Y., Pearce, J.A., 2007. The Dikili–Çandarlı volcanics,Western Turkey; magmatic interactions as recorded by petrographic and geochemical features. Turk. J. Earth Sci. 16, 493–522.

Yilmaz, Y., Genç, Ş.C., Gürer, O.F., Bozcu, M., Yılmaz, K., Karacık, Z., 2000. When did the western Anatolian grabens begin to develop? In: Bozkurt, E., Winchester, J.A., Piper, J.D.A. (Eds.), Tectonics ve Magmatism in Turkey ve the Surrounding Area. 173. Geological Society of London, Special Publication, pp. 353–384